JPRS-UMS-90-002
7 MARCH 1990

FOREIGN BROADCAST INFORMATION SERVICE

JPRS Report

Science & Technology

USSR: Materials Science

JPRS-UMS-90-002
7 MARCH 1990

SCIENCE & TECHNOLOGY

USSR: MATERIALS SCIENCE

CONTENTS

UDC 539.21-669.176

Influence of Structural State on Relaxation Properties of Titanium, Beryllium

18420207C Moscow IZVESTIYA AKADEMII NAUK SSSR: SERIYA METALLY No 2, Mar-Apr 89
(manuscript received 07 Dec 87), pp 146-149

[Article by A. K. Grigorev, N. G. Kolbasnikov, S. G. Fomin, R. Khenokh, Leningrad]

[Text] The performance of tests for stress relaxation in metals requires practically instantaneous loading, since stress relaxation begins simultaneously with an increase in load. Shock loading results in dynamic effects, distorting the results obtained. Therefore, the recording of fast relaxation processes in metal, which are observed upon cold deformation, is made more difficult. Standard tensile testing can be used to avoid these difficulties. We accept for this purpose the rheological model of an elastic–plastic material with hardening, which most fully reflects the processes occurring upon deformation of metallic materials. This model, consisting of an infinite number of elementary models as presented in Figure 1, can be described by the equation system[1]:

$$\begin{gathered}\sigma = 2G\left[e - \int_0^\infty\int_0^\infty p(\lambda, \tau)\, e_n\, d\lambda\, d\tau\right],\\ \dot{e}_n = 0,\ \left(\frac{1}{2}[e-(1+h)e_n]\ \ldots\ [e-(1+h)e_n]\right)^{1/2} \leqslant \tau,\\ \dot{e}_n \neq 0,\ \left(\frac{\tau}{v}+\lambda\right)\dot{e}_n + (1+h)e_n = e,\end{gathered} \tag{1}$$

where G represents the elastic properties of the metal, $G=\int_0^\infty\int_0^\infty F(\lambda,\tau)d\lambda d\tau$; F is a certain function of the arguments λ and τ, which has positive values, μ is the viscosity coefficient, G' is the rigidity, defining the linear deformation hardening of the metal; h is the hardening parameter; τ is the dimensionless elasticity limit of the model; λ is the relaxation time.

A metal has a discrete spectrum of relaxation times and spectrum of yield points $\{\lambda_{ijk}\}$ and $\{\tau_{ijk}\}$. Considering that in (1) the relaxation time and dimensionless yield points are independent, the joint probably density can be represented as $p(\lambda,\tau)=p_1(\tau)p_2(\lambda)$.

In body deformation with purely elastic change in volume a specific metal is defined by three constants μ, G, h and two functions $p_1(\tau)$ and $p_2(\lambda)$. Let us determine the parameters of a metal from experiments involving uniaxial extension. In this case equation system (1) becomes:

$$\sigma = E\left[e - \int_0^\infty \int_0^\infty p_1(\tau)\, p_2(\lambda)\, e_n d\lambda\, d\tau\right],$$
$$e_n = 0, \quad \tau \geqslant e,$$
$$\lambda \dot{e}_n + (1+h)\, e_n + \tau = e, \quad \tau < e. \tag{2}$$

With static extension of the metal the rate of viscous deformation can be ignored in comparison to the remaining terms and system (2) becomes:

$$\sigma = E\left[e - \int_0^\infty p_1(\tau)\, e_n\, d\tau\right],$$
$$e_n = 0, \quad \tau \geqslant e, \tag{3}$$
$$\tau + (1+h)\, e_n = e, \quad \tau < e.$$

Considering the second and third equations of system (3), the first equation can be written as

$$\sigma = E\left[e - \int_0^e \frac{1}{1+h}(e-\tau)\, p_1(\tau)\, d\tau\right]. \tag{4}$$

Differentiating (4) with respect to e, we obtain:

$$\frac{d\sigma}{de} = E\left[1 - \frac{1}{1+h}\int_0^e p_1(\tau)\, d\tau\right], \tag{5}$$

from which we can see that the elasticity modulus E can be determined as

$$\lim_{e \to 0} (d\sigma/de) = E. \tag{6}$$

The hardening h can be defined from the expression

$$\lim_{e \to \infty} (d\sigma/de) = Eh/(1+h). \tag{7}$$

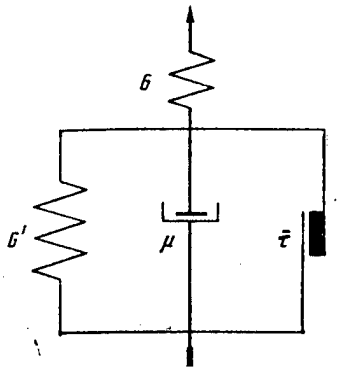

Figure 1. Model of Elastic–Viscous–Plastic Body with Hardening.

Thus, the tangent of the tensile curve slope in the steady state represents the hardening of the metal upon plastic deformation. Based on the second derivative

$$\frac{d^2\sigma}{de^2} = -\frac{E}{1+h}\, p_1(e) \tag{8}$$

we can determine the distribution density of $p_1(\tau)$. Thus, using expression (6)–(8), the static extension curve determines parameters E, h and $p_1(\tau)$.

To produce the function $p_2(\lambda)$ we must perform "dynamic" extension experiments, in which the deformation rate must be at least an order of magnitude higher than that used in static tests. For dynamic extension the deformation is determined at $e(t)=e_0 t$.

The equation for determination of stress is:

$$\sigma(t) = E\left\{\frac{h}{1+h}\, e_0 t + e_0 \int_0^{\infty} \frac{1}{(1+h)^2}\left[1-\exp\left(-\frac{1+h}{\lambda}\, t\right)\right]\times\right.$$
$$\left.\times\, p_2(\lambda)\int_0^{e_0 t} p_1(\tau)\, d\tau + \int_0^{e_0 t}\frac{\tau}{1+h}\, p_1(\tau)\, d\tau \int_0^{\infty}\exp\left(-\frac{1+h}{\lambda}\, t\right) p_2(\lambda) - \int_0^{e_0 t}\frac{\tau}{1+h}\, p_1(\tau)\, d\tau\right\}. \tag{9}$$

Let us introduce the symbols:

$$f(t) = \frac{\sigma(t)}{E} - \frac{h}{1+h} e_0 t + \int_0^{e_0 t} \frac{\tau}{1+h} p_1(\tau)\, d\tau,$$

$$y(t) = \int_0^{\infty} \lambda \left[1 - \exp\left(-\frac{1+h}{\lambda} t \right) \right] p_2(\lambda)\, d\lambda,$$

$$\varphi_1(t) = \int_0^{e_0 t} p_1(\tau)\, d\tau,$$

$$\varphi_2(t) = \int_0^{e_0 t} \frac{\tau}{1+h} p_1(\tau)\, d\tau.$$

Then equation (9) after a few transforms becomes:

$$y'(t) + \frac{e_0 \varphi_1(t)}{(1+h)\,\varphi_2(t)} y(t) = \frac{f(t)}{\varphi_2(t)} (1+h). \tag{10}$$

Solving linear heterogenous equation (10) numerically or analytically, we find the function *y(t)*. The function

$$\psi(t) = \frac{y''(t)}{1+h} = \int_0^{\infty} \exp\left(-\frac{1+h}{\lambda} t \right) p_2(\lambda)\, d\lambda \tag{11}$$

is called the relaxation function[2]. It was shown in [2] that the relaxation time distribution probability density can be determined by using the relaxation function $\psi(t)$ and the approximate equation

$$p_2(\lambda) = \left. \frac{d\psi(t)}{d(\lg t)} \right|_{t=\lambda}. \tag{12}$$

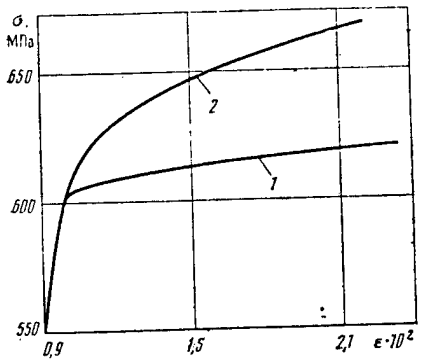

Figure 2. Static (1) and "Dynamic" (2) Curves of Extension for VT–1–0 Titanium, Obtained at Deformation Rates of $1 \cdot 10^{-4}$ and $2 \cdot 10^{-3}$ 1/s.

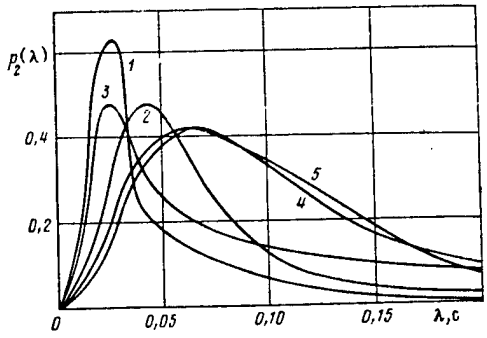

Figure 3. Probability Density of Relaxation Time Distribution for Titanium *(1–3)* and Beryllium *(4, 5)*: *1* and *2* — after annealing at 660 and 1050°C; *3* — after rolling at ϵ=30%; *4* — after annealing at 880°C; *5* — computed per equation (13).

Thus, by processing the results of static and dynamic tensile testing, we can determine all properties of the metal, representing its behavior upon plastic deformation.

In this work, we determined the relaxation time distribution density for titanium and beryllium and established their variation as functions of grain size and degree of deformation. These metals, particularly titanium, have minimum relaxation resistance, which facilitates the study of this phenomenon[3].

Test specimens were made of type VT–1–0 titanium and once–distilled beryllium with total impurity content about 1%. The titanium specimens were cold rolled to 0.4 mm thickness with intermediate annealing before testing. After rolling they were annealed at T=660±20 and 150±20°C to produce a mean grain size of ~30 and ~300 μm, respectively.

Beryllium specimens were hot rolled in soft steel envelopes to 0.1–0.15 mm thickness, then annealed at 880±20°C. After deformation and annealing, specimens were cut on an electric–spark cutter according to standard GOST 11701–66. Mechanical testing was performed on an Instron test machine at deformation rates of $1 \cdot 10^{-4}$ to $2 \cdot 10^{-1}$ s^{-1}.

Figure 2 shows the static and dynamic tensile test diagrams for titanium. Differentiation of the curves and determination of the intermediate function were performed graphically. The relaxation time distribution functions for titanium and beryllium (Figure 3) follow a log–normal distribution

$$p_2(\lambda) = \frac{A}{\lambda} \exp\left[-\frac{1}{2}\left(\frac{\ln \lambda - \mu_0}{\sigma_0}\right)^2\right], \tag{13}$$

where A is a coefficient selected from the normalization condition

$$\int_0^\infty p_2(\lambda)\, d\lambda = 1.$$

The distribution parameters μ_0 and σ_0 (table) were determined by a probability paper method. The function $p_2(\lambda)$ constructed from expression (13) is shown in Figure 3 (*5*). Conversion of the calculated function $p_2(\lambda)$, performed in reverse sequence using equations (13)–(2), makes it possible to construct a calculated extension curve for the metal studied (Figure 3). The maximum deviation of the calculated curve from the experimental curve did not exceed 0.7% for beryllium and 1.7% for titanium, indicating the good accuracy of the method used to determine the probability characteristics of the metal.

As we can see from Figure 3, the absolute value $\bar{\lambda}$ for the metals studied is small and for five–grain annealed titanium amounts to 0.025, for beryllium 0.1 s. The deformation of the metal does not significantly influence the relaxation properties (Figure 3, *1, 3*), whereas increasing grain size in titanium by an order of magnitude leads to an increase in $\bar{\lambda}$ by a factor of ~2, although the type of distribution remains unknown (figure 3, *1, 2*).

The method presented can be used to define both $\bar{\lambda}$ and the probability of stress relaxation to the required level within a given time limit. Assurance of stress relaxation directly in the deformation focus, as was shown in [4], can increase the gripability of the metal for cladding by rolling. During rolling, as during other technological processes, the maximum normal stresses in the metal will reach values significantly greater than the yield point, after which they relax to the yield point [3] as the external load is relieved.

Parameters of Titanium and Beryllium Relaxation Time Probability Distribution

Metal	A	μ_0	σ_0
Fine grain titanium after annealing at T=660°C	34,489	-3,23	1,035
Coarse-grain titanium after annealing at T=1050°C	23,706	-2,705	0,825
Fine grain cold rolled titanium, ϵ=30%	18,86	-2,125	1,41
Beryllium after annealing at T=870°C	0,168	-2,36	0,58

These studies have demonstrated that a significant fraction of the stresses accumulated in a metal in the process of deformation relax rather rapidly ($\bar{\lambda}$=0.025–0.1 s). If the stresses cannot relax before the load is released, the change in the sign of unrelaxed stresses from compressive to tensile, which occurs as a result of the recoil of spring G and G' where damper μ does not have time to operate (Figure 1) can cause the growth of microscopic cracks which are present in the metal and early failure.

Conclusions. 1. A method has been developed for determining the probability characteristics of a deformed metal — the probability distribution density of yield point and relaxation time from tensile tests.

2. For titanium and beryllium the relaxation time probability distribution density and yield point depend on the structural state of the metal: plastic deformation decreases the "quality" of $p(\lambda)$, while increasing grain size increases $\bar{\lambda}$ in comparison to fine-grain recrystallized metal.

REFERENCES

1. Fomin, S. G. "Mathematical Model of Elastic–Viscous–Plastic Metal Deformation Mechanism," Tr. LPI, No. 378, pp. 63, 1981.

2. Novik, A., Berri, B., Relaksatsionnye yavleniya v kristallakh [Relaxation Phenomena In Crystals], Moscow, Atomizdat Press, 1975.

3. Getsov, L. B., Borzdyka, A. M., Relaksatsiya napryazheniy v metallakh i splavakh [Stress Relaxation in Metals of Alloys], Moscow, Metallurgiya Press, 1978.

4. Karakozov, E. S., Soedineniye metallov v tverdoy faze [Solid–Phase Joining of Metal], Moscow, Metallurgiya Press, 1976.

UDC 669.046.46:669.231.5

Kinetics of Dissolution of Trans-Diaminodichloropalladium II in Batch Mode

18420223A Ordzhonikidze IZVESTIYA VYSSHIKH UCHEBNYKH ZAVEDENIY: TSVETNAYA METALLURGIYA in Russian No 5, Sep-Oct 88 (manuscript received 16 Jul 87), pp 23-27

[Article by G. N. Shivrin, I. I. Smirnov, I. A. Ratovskaya, Krasnoyarsk Institute of Nonferrous Metals; Department of Metallurgy of Heavy Nonferrous Metals; State Institute of Nonferrous Metallurgy

[Text] In refining it is frequently necessary to reduce the salts of platinum metals. One means of producing metals from their difficultly soluble compounds is electroreduction of oxide compounds of silver, copper, nickel, lead, and other metals[1-3]. In order to produce metallic palladium, we studied electrochemical reduction of trans-diaminodichloropalladium (II) (DADCP), which is difficulty soluble in aqueous solutions.

Studies were performed in an electrochemical cell with separation of the anode and cathode spaces by a diaphragm of porous titanium (Figure 1). The cathode space contained a mechanical agitator and titanium cathode. The electrolyte (0.4 dm^3) was poured in and the charge of DADCP was added (50 g). The electrolyte used was a solution of HCl (1-2 mol/dm^3). The cell was then heated to the desired temperature, thermostated and the current switched on.

DADCP is not very soluble in a hydrochloric acid solution, but does to some extent go over to soluble hydrogen tetrachloropalladate (II) (HTCP)

$$[Pd(NH_3)_2Cl_2]_{(т)}+4HCl_{(р)}\rightleftharpoons H_2[PdCl_4]_{(р)}+2NH_4Cl_{(р)}. \quad (1)$$

The dissolved HTCP is reduced on the cathode to metallic palladium

$$H_2[PdCl_4]+2\bar{e}=Pd+4H^++2Cl^-. \quad (2)$$

On the whole, the process of reduction of DADCP in the electrolytic cell consists of the following stages:

1. Convective-diffision movement of HCl from the solution to the surface of the DADCP particles.

2. Adsorption of HCl molecules on the surface of the DADCP crystals HCl(d), HCl(ads).

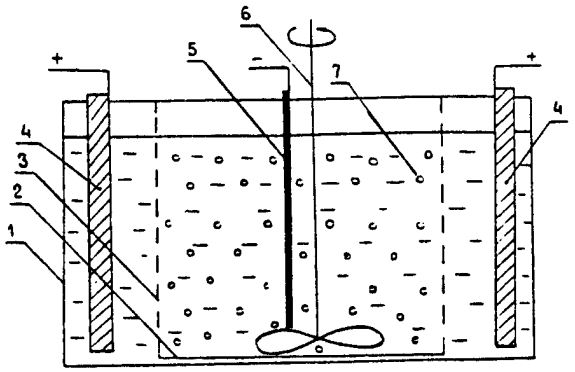

Figure 1. Diagram of Electrolyzer for Reduction of DADCP (II) in Chloride Solution. 1 — Body; 2 — titanium shell with catolyte; 3 — diaphragm of porous titanium; 4 — graphite anodes; 5 — titanium cathode; 6 — agitator; 7 — DADCP particles.

3. The chemical reaction between DADCP and HCl, accompanied by the formation of HTCP

$$[Pb(NH_3)_2]_{(т)}+4HCl_{(адс)}=H_2[PbCl_4]_{(адс)}+2NH_4Cl_{(адс)}. \qquad (3)$$

4. Desorption of HTCP molecules from the surface of the sediment particles

$$H_2[PbCl_4]_{(адс)}\rightleftharpoons H_2[PbCl_4]_{(р)}.$$

5. Diffusion-convective transfer of dissolved HTCP from the surface of the sediment particles to the solution.

6. Convective-diffusion transport of HTCP molecules to the surface of the cathode.

7. Electrode reaction of reduction of HTCP to metallic palladium.

Reaction (2) is irreversible, since the cathode space contains no oxidizer capable of dissolving metallic palladium in hydrochloric acid. Consequently, the influence of the reaction products of (2) and other dissolved substances on the electrochemical reduction of HTCP is not significant. However, reaction (2) may be inhibited by adsorbed HCl molecules or chloride ions.

If the process of reduction of DADCP is controlled by convective diffusion transport of the solvent (HCl) to the surface of the DADCP particles (Stage 1), the rate of dissolution of the sediment and transport of palladium into the solution should depend on the HCl concentration

$$v_1 = -VdC_{HCl}/4d\tau = VdC_{Pd}/d\tau = \kappa_1 \Delta C_{HCl}, \qquad (4)$$

where $k_1 = D_{HCl}a S_T/3\delta_1$, S_T is the surface of the DADCP particles, V is the volume of the solution (catolyte), D_{HCl} is the diffusion coefficient of HCl molecules in the water, δ_1 is the diffusion boundary layer near the surface of the DADCP particles, C_{HCl}, $(C_{HCl})_n$ is the concentration of HCl in the volume of the solution and on the surface of the DADCP.

With diffusion control of reaction (1) $C_{HCl} \gg (C_{HCl})_n$ and $\Delta C_{HCl} \approx C_{HCl}$. With slow adsorption of the HCl molecules on the surface of the DADCP particles (Stage 2), the rate of transition of palladium into the solution is

$$v_2 = \frac{VdC_{Pd}}{d\tau} = -\frac{S_T d\Theta_{HCl}}{4d\tau} = K_2' S_T C_{HCl}(1 - \Theta_{HCl}) - K_2'' S_T \Theta_{HCl}, \qquad (5)$$

where K_2', K_2'' are the rate constants of adsorption and desorption of HCl, Θ_{Hcl} is the degree of filling of the DADCP surface by adsorbed HCl molecules.

With high HCl concentration in the solution, Θ_{Hcl} is practically independent of the HCl concentration. Then equation (5) becomes

$$v_2 = VdC_{Pd}/d\tau = \kappa_2 S_T C_{HCl}, \quad \kappa_2 \neq f(C_{HCl}). \qquad (6)$$

In the case of a limiting chemical stage (Stage 3), the rate of transition of palladium into the solution also depends on the HCl concentration

$$v_3 = VdC_{Pd}/d\tau = \kappa_3 S_T (C_{HCl})_n, \qquad (7)$$

where k_3 is the rate constant of reaction (3).

With no diffusion limitations $(C_{HCl})_n = C_{HCl}$.

The concentration of HCl was fixed in excess and remained practically unchanged throughout the experiment. In experiments performed with an HCl concentration of 1

and 2 mol/dm^3 with otherwise equivalent conditions the slope of the line showing C_{Pd} as a function of τ should differ by a factor of two in accordance with (4)-(7). However, we established experimentally that the rate of dissolution of DADCP in the solution is independent of the HCl concentration. Consequently, stages 1-3 did not limit the rate of dissolution of DADCP in the hydrochloric acid solution.

The delay in desorption of HTCP molecules from the surface of sediment particles (Stage 4) increases the degree of filling of the molecule surfaces with HTCP and, consequently, the rate of desorption of the HTCP

$$v_4 = VdC_{Pd}/d\tau = S_T d\Theta_{Pd}/d\tau = \kappa_4 S_T \Theta_{Pd}. \quad (8)$$

The degree of filling of the surface with HTCP molecules depends on the HTCP concentration in the solution

$$\Theta_{Pd} = \kappa C_{Pd}^m,$$

where m varies from 1 at low palladium concentrations to 0 at higher concentrations.

The surface of the sediment particles changes over time ($S_T = k_T \tau^n$). The relationship between the concentration of palladium in the solution and the length of the experiment should be $\ln C_{Pd} = k\tau^{n+1}$ or

$$C_{Pd} = \exp(k\tau^{n+1}).$$

The experimental equation $C_{Pd} = f(\tau)$ (Figure 2*a*) presumes $n=0$, which is impossible for needle DADCP crystals. Therefore, desorption of HTCP molecules from the surface of the DADCP particles cannot limit the process of electroreduction of DADCP.

If the rate of dissolution of DADCP is limited by diffusion-convective transfer of HTCP from the surface of the DADCP particles into the solution (Stage 5), the transfer of palladium into the solution will follow the equation

$$v_5 = VdC_{Pd}/d\tau = \kappa_5[(C_{Pd})_n - C_{Pd}], \quad (9)$$

where $k_5 = D_{HTCP} S_T / \delta_5$,

— δ_5 is the thickness of the diffusion layer near a DADCP particle.

The thickness of the diffusion layer near a particle suspended in a flow of the solution is proportional to the radius of the particles [4] $\delta = a_1 R^n$ (n=2/3-1). The DADCP particles are needle shaped, and therefore their surface is proportional to their radius $S_T = a_2 R$($a_2 = 2\pi l$). Due to this, k_5 remains a constant quantity practically throughout the period of dissolution of the DADCP. The concentration of HTCP on the surface of a DADCP particle under conditions of slow diffusion is equal to the concentration of the saturated HTCP solution in a solution of a given HCl concentration and temperature.

Integration of equation (9) within limits from $\tau=0$ to τ and $C_{Pd}=0$ to C_{Pd} leads us to the expression

$$\ln\left[1-\frac{C_{Pd}}{(C_{Pd})_n}\right]=-\frac{\kappa_3}{V}\tau. \qquad (10)$$

Where

$$(C_{Pd})_n \gg C_{Pd} \quad \ln\left[1-\frac{C_{Pd}}{(C_{Pd})_n}\right]=-\frac{C_{Pd}}{(C_{Pd})_n}.$$

Then

$$\text{Тогда } C_{Pd}=\frac{\kappa_3}{V}(C_{Pd})_n\tau. \qquad (11)$$

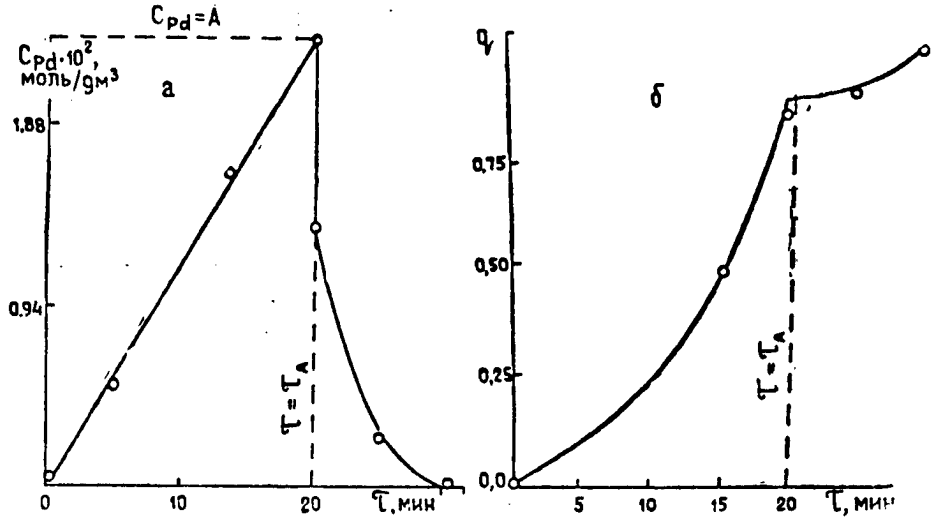

Figure 2. Dynamics of Change in Concentration (C) of Palladium in Catolyte (a) and Degree of Reduction of DADCP (II) in the Course of Electrolysis (b) at i=6000 A/m^2 and t=85° C.

Consequently, with diffusion limitation of the transfer of HTCP from the surface of a DADCP particle the palladium concentration in the solution should increase linearly

with time, while the rate of dissolution of the DADCP in the HCl and reduction of dissolved HTCP on the cathode are still different. This conclusion is confirmed experimentally (cf. Figure 2*a*).

The rate of reduction of dissolved HTCP on the cathode both in the case of diffusion limitation and in the case of delayed electron transfer of reaction (2) (Stages 6 and 7), is proportional to the palladium concentration in the solution

$$v_6 = -VdC_{Pd}/d\tau = \kappa_6 C_{Pd}, \tag{12}$$

$$v_7 = -VdC_{Pd}/d\tau = \kappa_7 C_{Pd}, \tag{13}$$

where $k_6 = D_{HTCPd} S_{cat}/\delta_{cat}$, S_{cat} is the working (immersed) surface of the cathode, δ_{cat} is the thickness of the diffusion layer at the cathode, k_7 is the rate constant of reaction (2).

Since neither k_6 nor k_7 depends on the concentration of palladium in the solution or the duration of the process, equations (12) and (13) can be combined

$$v_{6-7} = -VdC_{Pd}/d\tau = \kappa_{6-7} C_{Pd}. \tag{14}$$

The overall rate of transition of palladium into the solution is described by the equation

$$v = v_5 - v_{6-7} = VdC_{Pd}/d\tau = \kappa(A - C_{Pd}), \tag{15}$$

where

$$A = \kappa_5/\kappa(C_{Pd})_n, \quad \kappa = (\kappa_5 + \kappa_{6-7}).$$

Thus, the resultant change in palladium concentration in this solution is also linearly dependent on the duration of eletrolysis

$$C_{Pd} \approx kA\tau. \tag{16}$$

The cathodic reduction of the dissolved HTCP does not influence the nature of $C_{Pd} = f(\tau)$, and therefore the conclusion of limitation of the process as a whole by the stage of diffusion of HTCP molecules from the surface of the DADCP particles is valid as long as v_5 and v_{6-7} are different. The concentration of palladium in the solution reaches a maximum where $C_{Pd} = AA$.

The results of x-ray diffraction analysis of the sediment in the electrolyzer (mixture of DADCP and metallic palladium) indicates that the moment of equalization of the rates occurs when the DADCP is 85–90% reduced (Figure 2*b*). Then the rate of cathodic reduction of HTCP becomes the determining factor ($v_{6-7} \gg v_5$) in the overall rate of change of palladium concentration in the solution ($v \approx -v_{6-7}$). Further electrolysis results in full reduction of the DADCP sediment and a decrease in the concentration of palladium in the solution according to the exponential rule (cf. Figure 2)

$$C_{Pd} = A \exp\ [-\kappa_{6-7}(\tau - \tau_A)], \tag{17}$$

where τ_A is the moment of equalization of the rates of dissolution of DADCP and cathodic reduction of HTCP.

Thus, cathodic batch reduction of DADCP (II) in an electrolytic cell with intensive agitation in a chloride solution occurs in two stages: first, until 85-90% of the DADCP is dissolved, a slow stage involving diffusion-convective transfer of HTCP from the surface of the DADCP particles into the solution, followed by a stage of cathodic reduction of the dissolved HTCP.

REFERENCES

1. Lyamina, L. I., Korolkova, N. I., Gorbunova, K. M., "Cathodic Reduction of Lead Dioxide. 4.3. Structure of Lead Reduced From Its Dioxide," Elektrokhimiya, Vol 8, No 5, pp 651-654, 1972.

2. Lyamina, L. I., Tarasova, N. I., Gorbunova, K. M., "Kinetic Specifics of Electrochemical Reduction of Difficulty Soluble Compounds," Elektrodnyye protsessy i metody ikh izucheniya [Electrode Processes and Methods of Studying Them], Works of Second Republic Conference on Electrochemistry, Kiev, Naukova dumka Press, pp 99-102, 1978.

3. "Investigation of Process of Producing Metal Powders By Cathodic Reduction of Difficulty Soluble Compounds," Ye. F. Zavgorodnaya, yu. P. Rodak, T. Yu. Inytina, V. I. Lubyanova, Elektrodnyye protsessy i metody ikh izucheniya [Electrode Processes and Methods of Studying Them], Works of Second Republic Conference on Electrochemistry, Kiev, Naukova dumka Press, pp 273-275, 1978.

4. Levich, V. G., Fiziko-khimicheskaya gidrodinamika [Physical-Chemical Hydrodynamics], Moscow, Fizmatgiz Press, 700 pp, 1959.

UDC 66.094.3:546.98:513.71

Oxidizing Capacity of Chloride, Hydroxo Complexes of Palladium (II)

18420223B Ordzhonikidze IZVESTIYA VYSSHIKH UCHEBNYKH ZAVEDENIY: TSVETNAYA METALLURGIYA in Russian No 5, Sep-Oct 88 (manuscript received 07 Jul 87), pp 66-69

[Article by G. N. Shivrin, S. A. KOZLOVA, Krasnoyarsk Institute of Nonferrous Metals; State Institute of Nonferrous Metals

[Text] Complex compounds of palladium (II) can act as oxidizers in solutions, being themselves reduced to the metal. The reduction of complex compounds of platinum-group metals is a common approach to the production of metallic powders. Liberation of the metal from solution by reducing its compounds with hydrogen [1, 2], carbon monoxide [3, 4], the sulfite ion [5], formic acid [5] and other agents has been reported.

Complex compounds of palladium (II) have a planar configuration with 4 ligands [6]. Therefore, in general form the aqua-chloro-hydroxo complex compound of palladium (II) can be represented as $[Pd(H_2O)_{4-n-m}C_n(OH)_m]^{2-n-m}$. The coordination numbers for the ligands $CL^-(n)$ and $OH^-(m)$ may have values of 0 to 4. The complex compound of palladium (II) is reduced in the reaction

$$[Pd(H_2O)_{4-n-m}Cl_n(OH)_m]^{2-n-m} + 2e \rightleftarrows Pd + nCl^- + mOH^- + (4-n-m)H_2O. \quad (1)$$

The oxidizing capacity of a palladium (II) complex can be judged from the value of the electrode potential of the palladium in a solution of the composition in question:

$$\varphi_{[Pd(H_2O)_{4-n-m}Cl_n(OH)_m]^{2-n-m},Pd} = \varphi^0_{[Pd(H_2O)_{4-n-m}Cl_n(OH)_m]^{2-n-m},Pd} + \frac{RT}{2F}\ln\frac{a_{Pd}}{a_{Cl^-}^{n}\,a_{OH^-}^{m}\,a_{H_2O}^{4-n-m}}. \quad (2)$$

The oxidizing capacity of various complex compounds of palladium (II) can be conveniently compared under standard conditions. Since the standard potential of the electrode reaction (1) is not known for all possible compounds of palladium (II), the missing values of $\varphi^0_{[Pd(H_2O)_{4-n-m}Cl_n(OH)_m]^{2-n-m}Pd}$ can be computed.

Using the known values of constants for the formation of chloropalladate (II) ions from Cl^- and Pd^{2-} [7], as well as the standard potential of metallic palladium in the solution containing Pd^+ cations [8], let us compute the standard potential of a chloropaladate (II)-palladium electrode

$$\varphi^0_{Pd\,(H_2O)_{4-n}Cl_n]^{2-n}/Pd} = \\ = \varphi^0_{[Pd\,(H_2O)_4]^{2+}/Pd} + \frac{RT}{2F} \ln \beta, \qquad (3)$$

where β is the equilibrium constant of the reaction of dissociation of the chloropalladate (II) ions

$$[Pd\,(H_2O)_{4-n}\,Cl_n]^{2-n} + nH_2O = \\ = [Pd\,(H_2O)_4]^{2+} + nCl^-. \qquad (4)$$

The results of the calculation are presented in the Table.

Redox Capacity of Complex Palladium (II) Compounds

Complex Compounds	$\varphi^0_{complex\ Pd}$, V
$[Pd\,(H_2O)_4]^{2+}$	0,987 [8]
$[Pd\,(H_2O)_3Cl]^+$	0,86
$[Pd\,(H_2O)_2Cl_2]$	0,765
$[Pd\,(H_2O)\,Cl_3]^-$	0,69
$[PdCl_4]^{2-}$	0,645*
$[Pd\,(H_2O)_3OH]^+$	0,64
$[Pd\,(H_2O)_2Cl\,(OH)]$	0,57**
$[Pd\,(H_2O)\,Cl_2\,(OH)]^-$	0,52**
$[PdCl_3\,(OH)]^{2-}$	0,48
$[Pd\,(H_2O)_2\,(OH)_2]$	0,29
$[Pd\,(H_2O)\,Cl\,(OH)_2]^-$	0,29**
$[PdCl_2\,(OH)_2]^{2-}$	0,29**
$[Pd\,(H_2O)\,(OH)_3]^-$	0,235
$[PdCl\,(OH)_3]^{2-}$	0,235**
$[Pd\,(OH)_4]^{2-}$	0,205

* Reported value 0.62 V [8].
** Graphic estimate.

Using known data on the hydrolysis constants of the $[Pd(H_2O)_4]^{2+}$ cation [9], let us now use equations (3) to compute the standard potentials of the hydroxopalladate (II)-palladium electrode (cf. table). In this case the β-equilibrium constant of the hydrolysis reaction

$$[Pd(H_2O)_4]^{2+} \rightleftarrows [Pd(H_2O)_{4-m}(OH)_m]^{2-m} + mH^+. \quad (5)$$

To compute $\varphi^0_{[Pd(H_2O)_{4-n-m}Cl_n(OH)_m]^{2-n-m}Pd}$ requires data on the hydrolysis of the chloropalladate (II) ions

$$\varphi^0_{[PdCl_{4-m}(OH)_m]^{2-}/Pd} = \varphi^0_{[PdCl_4]^{2-}/Pd} - \frac{RT}{2F} \ln K, \quad (6)$$

where K is the equilibrium constant of the reaction of hydrolysis of the chloropalladate (II) ions:

$$[PdCl_4]^{2-} + mOH^- \rightleftarrows [PdCl_{4-m}(OH)_m]^{2-} + mCl^-. \quad (7)$$

Hydrolytic equilibria in chloride solutions of palladium (II) were studied in [10, 11]. The approximate value of K was computed for m=1. The constants of hydrolysis of $[PdCl_4]^{2-}$ in subsequent stages are unknown. Data on the hydrolysis of mixed aqua chloropalladate (II) ions are also not available. The replacement in the $[Pd(H_2O)_4]^{2+}$ molecule of water by a hydroxide ion yields the linear variation of $\varphi^0_{[Pd(H_2O)_{4-m}(OH)_m]^{2-m}/Pd}$ as a function of number of OH^- ligands in the coordination sphere of the complex within limits of m=0–2 (Figure, *a*). A further increase in m to 4 leads to a comparatively small change in the potential.

To construct the variation of $\varphi^0_{[PdCl_{4-m}(OH)_m]^{2-}/Pd}$ as a function of the number of substituted Cl^- ligands, three points of the five possible points were placed on the hydroxide ions. The potentials $\varphi^0_{[PdCl_2(OH)_2]^{2-}/Pd}$ and $\varphi^0_{[PdCl(OH)_3]^{2-}/Pd}$ were unknown. These potentials can be estimated using the fact of approximate equality of the energy manifestations of substitution in the coordination sphere of palladium (II) upon replacement of a water molecule and a chloride ion with the OH^- ligand.

Thus, substitution of an OH^- for an individual Cl^- ligand in the complex $[Pd(H_2O)_3Cl]^+$ and H_2O in the complex $[Pd(H_2O)Cl_3]^-$ yields an emf of the substitution reaction of 0.22 and 0.21 V. This indicates that substitution of hydroxide ions for two Cl^- ligands in the complex $[Pd(H_2O)_2Cl_2]$ and two H_2O ligands in the same complex should yield approximately the same emf of these two substitution reactions. Then $\varphi^0_{[PdCl_2(OH)_2]^{2-}/Pd} \approx \varphi^0_{[Pd(H_2O)_2(OH)_2/Pd} = 0.21$ V, and the replacement in the complex $[PdCl_4]^{2-}$ ligands of Cl^- by OH^- also yields the linear variation of $\varphi^0_{[PdCl_{4-m}(OH)_m]^{2-}/Pd}$ within the limits m=0–2. Further replacement of Cl^- ligands by hydroxide ions (m>2) is accompanied by agreement of the potentials $\varphi^0_{[PdCl_{4-m}(OH)_m]^{2-}/Pd}$ and $\varphi^0_{[Pd(H_2O)_{4-m}(OH)_m]^{2-m}/Pd}$. For m=4 this is unconditional, for m=3 it is obvious.

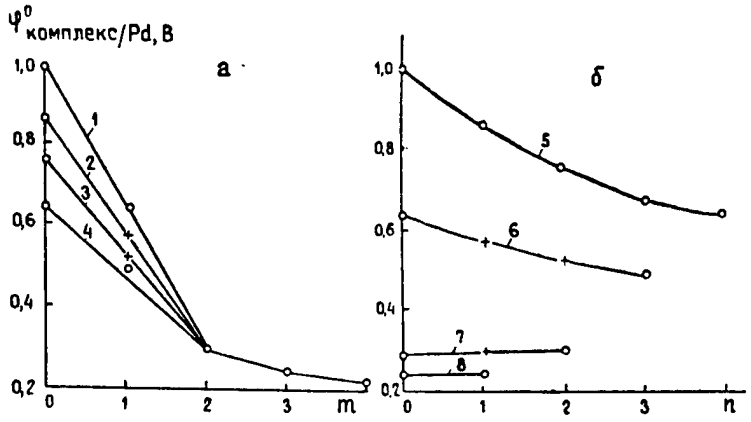

Variation of $\varphi^0_{complex/Pd}$ as a Function of Number of OH^- Ligands (m) — *a* and Cl^- Ligands (n) — *b* in Composition of Complex Palladium (II) Compound.

1—$[Pd(H_2O)_{1-m}(OH)_m]^{2-m}$,
2—$[Pd(H_2O)_{3-m}Cl(OH)_m]^{1-m}$,
3—$[Pd(H_2O)_{2-m}Cl_2(OH)_m]^{-m}$,
4—$[PdCl_{4-m}(OH)_m]^{2-}$,
5—$[Pd(H_2O)_{4-n}Cl_n]^{2-n}$,
6—$[Pd(H_2O)_{3-n}Cl_n(OH)]^{1-n}$,
7—$[Pd(H_2O)_{2-n}Cl_n(OH)_2]^{-n}$,
8—$[Pd(H_2O)_{1-n}Cl_n(OH)_3]^{-1-n}$.

o — experimental and calculated data; x — most probable values determined by graphic interpolation.

Based on what we have said, we can assume that replacement of H_2O and Cl^- ligands by hydroxide ions in complex $[Pd(H_2O)_{4-n}Cl_n]^{2-n}$-type compounds also yields linear variation of $\varphi^0_{[Pd(H_2O)_{4-n-m}Cl_n(OH)_m]^{2-n-m}/Pd}$ as a function of m where m=0-2 (cf. Figure, *a*). This allows approximate graphic determination of the most probable values of the potentials, which are presented in the table.

If we analyze the influence of replacement of a water molecule in the coordination sphere of palladium (II) by chloride ions (cf. Figure, *b*), we see that the variation of $\varphi^0_{[Pd(H_2O)_{4-n-m}Cl_n(OH)_m]^{2-n-m}/Pd}$ as a function of n changes monotonically, which allows us to correct the values of the potentials as determined from the diagram of Figure *a*.

Analysis of the variation in oxidating capacity of various complex palladium (II) compounds as a function of their structure leads us to the following conclusions:

1. The maximum oxidizing capacity is that of hydrated palladium (II).

2. Replacement of coordination water with any ligand (Cl^- or OH^-) decreases the oxidizing capacity of the complex palladium (II) compound formed in comparison to $[Pd(H_2O)_4]^{2+}$.

3. Hydrolysis of chloropalladate (II) ions decreases their oxidizing capacity.

4. By using various reducing agents it is possible to isolate metallic palladium from various complex compounds which are dissolved under these conditions.

REFERENCES

1. Beketov, N. N., Sbornik izbraniykh proizvedeniy [Selected Works], Moscow, Acad. Sci. USSR Press, 425 pp, 1954.

2. Ipatev, V. V., Tronev, V. G., Doklady AN SSSR, Vol 11, No 1, pp 29-32, 1935.

3. Spitsyn, V. I., Znamenskiy, I. V., Fedosyev, I. V., Doklady AN SSSR, Vol 181, No 3, pp 617-619, 1968.

4. Golodov, V. A., Kutyukov, G. G., fasman, A. V., Sokolskiy, D. V., ZhNKh, Vol 9, No 10, pp 2319-2323, 1964.

5. French Patent No. 2168119, "Methods of Producing Complex Acid Sulfate of Sodium and Colloidal Platinum," Published 23 Feb 73.

6. Grinberg, A. A., Vvedeniye v khimiyu kompleksnykh soedineniy [Introduction to Chemistry of Complex Compounds], Moscow, Khimiya Press, 632 pp, 1966.

7. Ginzburg, S. I., Yezerskaya, N. A., Prokofeva, I. V., et al., Analiticheskaya khimiya platinovykh metallov [Analytic Chemistry of the Platinum Metals], Moscow, Nauka Press, 614 pp, 1972.

8. Spravochnik po elektrokhimii [Electrochemistry Handbook], Edited by A. M. Sukhotin, Leningrad, Khimiya Press, 488 pp, 1988.

9. Nazarenko, V. a., Antonovich, V. P., Nevskaya, V. P., Gidroliz ionov metallov v razbavlennykh rastvorakh [Hydrolysis of Metal Ions in Dilute Solutions], Moscow, Atomizdat Press, 172 pp, 1979.

10. Grainberg, A. A., Kiselev, N. V., ZhNKh, Vol 3, pp 1804, 1958.

11. Kazakova, V. I., Ptitsyn, B. V., ZhNKh, Vol 12, pp 620, 1967.

Structure Formation in Combined Multilayer Coating

907D0028A Kishinev ELEKTRONNAYA OBRABOTKA MATERIALOV in Russian No 4, Jul-Aug 89 pp 17-19

[Article by L. I. Pupan, V. I. Kononenko, A. M. Kotlyar, L. V. Zhivkova, Kharkov: "Structure Formation in a Combined Multilayer Coating"]

[Text] Requirements for modern materials are often met only through the use of the latest advances in modern coating technology. An example is a multilayer composite coating on stainless steel.

Stainless steel 12Kh18N10T may be considered the most common material in dental practice, but the unacceptable medical, biological, and aesthetic properties of the design of metal dental prostheses (MZP) made of this material necessitate the application of multilayer coatings on its surface.

The object of this work was to investigate the structural features of a multilayer composite coating and the effect of manufacturing operations on phase-structure transformations in it. The object of study was a composite consisting of Ni, Ti, Ti+TiN, and TiN applied to specimens of two dimensional series (A - 5 x 50 x 0.1 x 10^{-3} m^3; B - 25 x 10 x 10 x 10^{-3} mm^3) of stainless steel 12Kh18N10T. The first layer, applied to the base, was produced by electroless nickel-plating[1]. The purpose is to protect soldered joints in the MZP structure from the effects of the high temperatures that develop when subsequent coatings are applied. Chemical precipitation processes make it possible to produce even coatings on parts with the most complicated shape, such as MZPs. In addition, during electroless nickel-plating the micropores measuring up to whole microns that are found in cast parts, most often in the soldered joints of assembled protheses, grow together.

The second layer, an intermediate titanium layer, is applied by vacuum plasma spraying[2]. This layer (0.3-0.8·10^{-6} m thick) is a transition between the temperature-resistant nickel and the protective-decorative titanium nitride layer. It provides good bonding with the crystalline nickel layer and partially relaxes stresses caused by the difference in these layers' coefficients of thermal expansion. The last two layers, which have protective-decorative functions, are produced by vacuum plasma spraying.

The structure of the layers was studied with a UEMV-100K microscope by two-stage replica method and radiography. It was established that the temperature at which the quasi-amorphous Ni-P film enters a crystalline state, described by an increase in hardness and an improvement in adhesion for the

free film separated from the base are different from the temperature of the film coating on the stainless steel's surface. For the free film, the transformation temperature was close to 670 K; for the film on the surface when adhesion is good, 620 K. Holding time in both cases was 30 min. In addition, the structural state of the coating turned out to be sensitive to the base's thickness. This conclusion was made on the basis of electron microscopy and radiography studies of a chemically precipitated Ni-P coating on specimens of different thicknesses and sizes. The coating for A specimens had a basically fine-grained structure. All microdiffraction patterns contained highly blurred circular, almost halo-like, lines. In these specimens, both overall diffraction and microdiffraction indicate structural nonuniformity. All electron diffraction patterns can be broken down into two groups. One is characterized by GTsK [face-centered crystal] phase lines, whose interplanar distances are greater than those for pure nickel and change over the surface of the same specimen. This phase may be interpreted as the solid solution of variable composition of phosphorus in nickel. The period of the lattice of this solution changes over the specimen within $(3.68\text{-}3.89)\cdot10^{-10}$ m; $a_{Ni}=3.517\cdot10^{-10}$ m, i.e. $\Delta a_{Ni}=(0.16\text{-}0.37)\cdot10^{-19}$ m.

Electron diffraction patterns for the other group contain lines belonging to two phases. In one, the lattice period is increased compared to pure nickel, i.e. it is a solid solution of phosphorus in nickel, like for the first group. The second phase may be identified as Ni_3P. Furthermore, the electron diffraction patterns for this have narrow lines for both phases, which indicates the inception of the crystallization process. Consequently, the structure of the nickel coatings is heterogeneous: along with almost amorphous areas, there are areas where crystallization has occurred. The surface layer of these coatings is characterized by two kinds of areas differing in chemical composition (one- and two-phase). The concentration of the solid solution of phosphorus in the nickel changes both in macro- (10^{-4}) and in microregions (10^{-8} m).

Nickel coatings on B specimens have a different structure. First, the coating structure is homogeneous over the surface. Second, decoded electron diffraction patterns revealed the presence of three crystallographic phases: Ni, Ni_2P, Ni_3P, with the following intensity distributions: $J_{Ni2P}>J_{Ni}>J_{Ni3P}$. The change in the nickel lattice period compared to tabular values[3] is negligible and amounts to $\Delta a_{Ni}\doteq0.07\text{-}0.09\cdot10^{-10}$ m. This is considerably lower than for A specimens. Microelectron diffraction patterns of the nickel coating for these specimens have multiple points with a fine structure. This is probably related to both the substructure and the shape of the crystal particles and the presence of imperfections and strains in the crystal lattice. Analysis of the fine structure makes it possible to talk about the presence of twin layers and stacking defects in the nickel layer.

Study of the bright-field images showed that the Ni_3P phase segregrations are needle-shaped and measure about 10^{-7} m and that the distribution over the surface is even.

We paid a great deal of attention to the structural state of this sub-layer because of the possibility of setting and regulating macrostresses in it by changing precipitation process parameters[4].

Electron microscopy of the intermediate titanium layer showed that there were no significant changes in the phase state or structure of this layer, either after heat treatment or after ion bombardment.

Let us consider the phase and structural state of the protective-decorative TiN layer with a Ti+TiN sub-layer. After treatment, the multilayer composite was separated from the base, the nickel layer was removed by chemical etching, and the remaining Ti, Ti+TiN, and TiN layers were submerged by ion etching in a VUP-4 setup. The results confirmed that the phase composition of this layer is heterogeneous over its thickness. This heterogeneity was artificially created to lower thermal residual stresses between the layers of the composite and to improve adhesion characteristics.

The optimum nitrogen content in the coating was defined by product requirements (microhardness, color, adhesion, residual stresses, etc.). Unfortunately, precise determination of the stoichiometric composition with electron diffraction patterns is impracticable[5]. The protective-decorative titanium nitride layer has an extremely small-crystal structure and a high level of stresses, which is caused by the unevenness of condensation process and structural heterogeneity. Electron microscopy revealed that these film coatings contain a crystal phase of titanium nitride. The nucleation of elongated crystallites takes place in an amorphous matrix. The crystallization process is uneven over the surface of the specimen, as indicated by the wide range of crystal sizes from 10^{-7} to $5 \cdot 10^{-6}$ m.

Metallographic study of the sprayed surface after scratching with a diamond pyramid indicates that both the nickel layer's transition from a quasi-amorphous state to a crystal and the nucleation of titanium nitride crystallites improve the coating's adhesive properties.

Conclusions. 1. The multilayer coating that was studied does not require additional heat treatment in order for the unstable quasi-amorphous nickel to enter into a crystal state, since this is ensured during ion bombardment, when the part is heated and the surface is modified through the formation of structures with increased density and good adhesion.

2. Regardless of base thickness and the characteristics of the intermediate layers, the protective-decorative titanium nitride coating is formed by the nucleation of the titanium nitride crystal phase in an amorphous-like matrix.

3. Sheet layers of nickel, titanium and a sub-layer of Ti+TiN in the range of thicknesses studied, which relax mechanical stresses in a multilayer coating, totally eliminate micro- and macrocracks in the outer decorative-protective layer.

References

1. S. A. Vishenkov, "Khimicheskiye i elektroliticheskiye sposoby osazhdeniya metallopokrytiy" [Chemical and Electrolytic Methods of Metal Coating Deposition]. Moscow, 1975.

2. A. M. Dorodkov, V. A. Petrosov, "On the Physical Principles of Vacuum Plasma Manufacturing Devices," ZhTF, 1981, 51, No. 3, pp. 504-524.

3. L. S. Mirkin, "Spravochnik po rentgenostrukturnomu analizu podkristallov" [Handbook on Radiostructural Analysis of Subcrystals]. Moscow, 1961.

4. P. G. Norris, "Electroforming Precision on Design," ENGINEERING MATERIALS AND DESIGN, 1981, 25, No. 6, pp. 24-27.

5. G. Beensh-Marchurcka, et al., "Wlasnosii cienkich warstu azotku tytanu," PLACE NAUKOWE INSTYTUT TECHNOLOGY ELECKTRONOWY, 1979, No. 23, pp. 1-77.

Structure of Iron-Alloy-Based Electrochemical Composite Coatings

907D0028B Kishinev ELEKTRONNAYA OBRABOTKA MATERIALOV in Russian No 4, Jul-Aug 89 pp 19-22

[Article by Zh. I. Bobanova, G. V. Guryanov, S. P. Sidelnikova, Kishinev: "Structure of Iron-Alloy-Based Electrochemical Composite Coatings"]

[Text] The development and advancement of the branches of technology are linked to the use of new heat-resistant materials. Electrochemical composite coatings (KEP) are important among these materials.

The object of this work was to study the effect of heat treating KEPs on their structure and microhardness. KEPs based on Fe-Co and Fe-Mn alloys were produced from electrolyte suspensions of the following composition: 500 g/liter of iron chloride, 100 g/l of cobalt sulfate, (pH 0.8-1.0, T=50°C), and 150 g/liter of iron fluorosilicate, 240 g/liter manganese sulfate, 130 g/liter ammonium sulfate (pH=1.6-1.8, T=50°C) -- containing a dispersed phase of Al_2O_3, B_4C, SiC, SiO_2, MoS_2 in a quantity of 50-150 g/liter (the concentration of MoS_2 particles varied within 3-9 g/liter). Particles of various grades were used to prepare the suspension: Al_2O_3, M-2, M-7, M-14; B_4C, M-14, M-40; SiC, M-3, M-14, M-28. Precipitation current density was 10-20 A/dm^2.

The phase transformations in electrolytic precipitates were studied by radiostructural analysis. Diffractions patterns were filmed on a URS-50 IM in Co radiation[1]. Fine structure parameters (size of mosaic blocks, micro-distortions, and dislocation density) were calculated according to the procedure in reference 2.

Coating microhardness was measured on a PMT-3 microhardness gauge after heat treatment at 200, 300, 400, and 500°C.

The size of the areas of coherent scattering of KEP based on iron-cobalt and iron-manganese alloys depends on the nature and content of dispersed particles in the coatings and their size. It was established that the size of the mosaic blocks crosses maximum as the concentration of dispersed particles of aluminum oxide increases from 50 to 100 g/liter in electrolyte suspensions for producing iron-cobalt and iron-manganese KEPs increases. Introducing dispersed particles of silicon oxide into the iron-manganese alloy reduced the size of the KEP mosaic blocks by more than half compared to the coating without dispersed silica.

The size of micro-distortions in the iron-manganese alloy crystal lattice depends on the nature and quantity of dispersed particle inclusions. The density of KEP dislocations changes antipathically to the size of the blocks as particle concentration changes.

When sub-microstructure was studied as a function of specimen heating temperature, the following features were observed. The temperature profile for the mosaic blocks of electrolytic iron coatings had maxima in the 200-250 and 550-600°C ranges. When the iron-cobalt alloy was heated to 350-450°C (without inclusion of dispersed particles) the size of the coating mosaic blocks was almost unchanged. If temperature rose further, the size of alloy sub-grains grew abruptly, apparently because of the formation of angular boundaries between the blocks and the increase in recrystallization "nucleus" migration speeds.

When dispersed particles were introduced into the matrix, the size of the mosaic blocks dropped sharply as temperature rose in the 300-350°C for iron-manganese-based KEPs with aluminum oxide, boron carbide, silicon carbide particles; and in the 500-550°C range for iron-cobalt-aluminum oxide KEPs.

Radiography revealed that by the time the recrystallization process began, the microdistortions detected in the KEP based on iron-manganese had diminished.

The relationship of the density of iron-cobalt alloy dislocations and the KEP based on it with dispersed aluminum oxide, boron carbide, and silicon carbide particles to temperature has a maximum whose appearance is probably due to the interaction of the moving dislocations with particles, the change in the density of dislocations around the particles., and the effective distance between them[3]. Note that dislocation density of the alloy without the dispersed phase is an order of magnitude higher than in coatings produced from electrolyte suspensions.

The process by which electrolytic iron precipitates loses strength is subordinate to ordinary thermodynamic principles, i.e. as dislocation and micro-distortion density increases, recrystallization begins at reduced temperatures, and as the content of dispersed inclusions in the coatings increases, the onset of recrystallization is shifted toward the higher temperature range.

The data correlate well with measurements of the microhardness of heat treated KEPs. The turn on the curves for the temperature-dependence of the microhardness logarithm corresponds to the temperature at which loss of strength begins, when there is a drop in hardness, modulus of elasticity, and other strength characteristics. It is possible that there is a changeover from a shear strain mechanism caused by dislocation creep to diffusion strain caused by the ascent of dislocations[4] near the coating recrystallization temperature. Analysis of the curves relating $\ln H_{\mu}$ and t showed that heat treatment at 100-500°C stabilizes the microhardness of iron-cobalt and iron-manganese alloys with dispersed aluminum oxide, boron carbide, and silicon carbide particles.

The introduction of dispersed boron carbide and aluminum oxide particles into iron-cobalt and iron-manganese alloys in a quantity of 10-12 weight percent

and the heat treatment of these coatings to 400-500°C stabilizes their structure, and microhardness changes only slightly. This ensures the operating reliability and toughness of these materials and makes it possible to recommend them for the production of creep- and scaling-resistant coatings operating at 300-400°C.

The coatings' strengthening action may be explained by the effect of the blocking mechanism, when the coating acts as a barrier keeping the dislocations away from the elastic repulsion surface between the dislocations in the substrate and the coating with a shear modulus greater than that of the substrate, as well as the coating's suppression of Frank-Reed surface sources[5].

References

1. A. S. Umanskiy, "Fizicheskiye osnovy metallovedeniya" [Physical Basis of Metals Science]. Moscow, 1955.

2. Ya. D. Vishnyakov, A. N. Ivanov, M. N. Peregudov, KRISTALLOGRAFIYA, 1968, 13, No. 6, p. 1023.

3. V. K. Grigorovich, "Svoystva i primeneniye zharoprochnykh splavov" [Properties and Application of Scale-and-Creep-Resistant Alloys]. Moscow, 1966, pp. 58-65.

4. "Rol dislokatsiy v uprochnenii i razrushenii metallov" [Role of Dislocations in Strengthening and Failure of Metals], ed. by V. S. Ivanova. Moscow, 1965.

Calculating Temperature Field of Substrate-Coating System Exposed to Heat From Plasma Flow of Variable Power

907D0028C Kishinev ELEKTRONNAYA OBRABOTKA MATERIALOV in Russian No 4, Jul-Aug 89 pp 22-25

[Article by Zh. A. Mrochek, A. K. Vershina, S. D. Izotova, Minsk:
"Calculating the Temperature Field of a Substrate-Coating System Exposed to Heat from a Plasma Flow of Variable Power"]

[Text] Vacuum coating processes are now common: ion atomization, precipitation in a plasma of electric discharges, ion precipitation, and plasma accelerator precipitation[1]. This last process is the furthest developed and used because of the high quality of coatings applied from different materials by direct synthesis without the output of byproducts[2]. In modern vacuum metallization equipment, coatings are usually applied onto moving substrates typically rotating either around their own axes or around that of the carousel or in planetary motion. During rotation the substrate passes through zones with different ion current densities. The density of the thermal flow to the condensation surface therefore depends on the location of the substrate in the unit's vacuum chamber. In this regard, study of the temperature fields formed in a substrate-coating system exposed to the thermal action of a plasma flow of variable power is interesting for many engineering and technical applications.

This article reviews problems in modeling the temperature field of a substrate and coating during coating precipitation by condensation of plasma flows in a vacuum with ion bombardment (KIB method)[3] with the following assumptions. The substrate-heating system is heated by a heat flow evenly distributed over the condensation surface. During the ion cleaning which precedes condensation and is one of the fundamental stages of substrate surface preparation before coating application[3], a thin (ξ_0) transitional layer forms on the substrate as a result of ion implantation. The thermophysical properties of this layer differ slightly from such coatings. Substrate rotation around the carousel axis at speed w begins at time $\tau>0$, when the distance between the cathodes and the substrate is minimum. Then the density of the heat flow to the substrate surface may be described by a periodic function like

$$q(\tau)=b_0+b_1\cos w\tau-b_2\,|\sin w\tau|, \qquad (1)$$

where τ is the time to generate coating material by a vacuum arc cathode spot; b_0, b_1, b_2, coefficients depending on the electrical parameters of the coating precipitation process (arc discharge current I_g, substrate shift potential u_p,

plasma flow focusing current I_f) and the coating material's thermophysical properties.

Assuming the thermophysical properties of the coating and substrate materials and disregarding thermal losses to radiation because of their small size, we can present the mathematical model of the heat transfer process in the substrate-coating system in terms of the increase in coating thickness as

$$\frac{\partial t_1(x,\tau)}{\partial \tau} = a_1 \frac{\partial^2 t_1(x,\tau)}{\partial x^2} \quad (-\xi(\tau) < x < 0), \tag{2}$$

$$\frac{\partial t_2(x,\tau)}{\partial \tau} = a_2 \frac{\partial^2 t_2(x,\tau)}{\partial x^2} \quad (0 < x < l), \tag{3}$$

$$t_1(x,0) = t_2(x,0) = t_0, \tag{4}$$

$$\lambda_1 \frac{\partial t_1(-\xi(\tau),(\tau)}{\partial x} = -q(\tau), \tag{5}$$

$$t_1(0,\tau) = t_2(0,\tau), \tag{6}$$

$$\lambda_1 \frac{\partial t_1(0,\tau)}{\partial x} = \lambda_2 \frac{\partial t_2(0,\tau)}{\partial x} = -\varphi(\tau), \tag{7}$$

$$\frac{\partial t^2(l,\tau)}{\partial x} = 0. \tag{8}$$

Here the subscript i=1 denotes values pertaining to the coating; i=2, to the substrate; $t(x,\tau)$, temperature at point x at time τ; a and λ, coefficients of thermal diffusivity and thermal conductivity; $\xi=\xi_0+\omega\tau$, ω is the rate at which coating thickness increases; $\phi(\tau)$, density of the thermal flow at the coating-substrate contact; t_0, initial temperature of the transition layer and the substrate; l, substrate thickness.

The thermal task in this statement is nonlinear. Therefore its solution can be found most simply using numerical or approximation methods. Since most numerical methods require significant amounts of computer and human time, we will solve problems (2)-(8) with Goodmen's approximate integral method[5]. We will approximate the coating's and substrate's temperature profiles with second-degree polynomials of x:

$$t_i = \sum_{j=0}^{2} A_{ji} x^j, \tag{9}$$

where coefficients A_{ij} (i=1,2), which are in general functions of time τ and take the following form

$$A_{10} = Y - \frac{\xi}{2\lambda_1}(\varphi + q), \quad A_{11} = -\frac{1}{\lambda_1}\varphi, \quad A_{12} = \frac{1}{2\lambda_1 \xi}(q-\varphi),$$
$$A_{20} = Z + \frac{l}{2\lambda_2}\varphi, \quad A_{21} = -\frac{1}{\lambda_2}\varphi, \quad A_{22} = \frac{1}{2\lambda_2 l}\varphi, \tag{10}$$

where $Y=t_1(-\xi,\tau)$, $Z=t_2(l,\tau)$ are the temperatures of the free surfaces of the coating and substrate.

Let us establish the relationship between temperatures Y and Z and coating precipitation time. Integrating the differential equations for thermal conductivity (2) and (3) in terms of x, we will write thermal balance equations for the constituents of the substrate-coating system. By calculating these integrals, we will obtain ordinary differential equations

for determining Y and Z:

$$Y'-m(\tau)=0, \tag{11}$$
$$Z'-n(\tau)=0, \tag{12}$$

where

$$m(\tau)=(a_1)(\lambda_1\xi) + (\xi'/3\lambda_1)(\phi+2q) + (\xi/6\lambda_1)(\phi'+2q'),$$

$$n(\tau)=(1/\lambda_2 t)(a_2\phi - l^2\phi'/6).$$

The solution to equations (11) and (12) takes the form

$$Y=t_0-\frac{a_1}{\lambda_1}\int_0^\tau \frac{1}{\xi}(q-\varphi)d\tau+\frac{\omega}{3\lambda_1}\int_0^\tau(\varphi+2q)d\tau+$$
$$+\frac{\xi}{6\lambda_1}(\varphi+2q). \tag{13}$$

$$Z=t_0-\frac{l}{6\lambda_2}\varphi+\frac{a_2}{\lambda_2 l}\int_0^\tau \varphi d\tau. \tag{14}$$

On the basis of conjugation condition, we obtain the integral equation for determining the density of thermal flow $\phi(\tau)$ on the coating-substrate contact

$$\int_0^\tau\left\{\left(\frac{a_1}{\lambda_1\xi}-\frac{\omega}{3\lambda_1}+\frac{a_2}{\lambda_2 l}\right)\varphi-\left(\frac{a_1}{\lambda_1\xi}+\frac{2\omega}{3\lambda_1}\right)q\right\}\times$$
$$\times d\tau=-\frac{\xi}{6\lambda_1}q-\frac{1}{3}\left(\frac{\xi}{\lambda_1}+\frac{l}{\lambda_2}\right)\varphi. \tag{15}$$

Equation (15) was solved numerically by grid method with an algorithm similar to that in references 6 and 7. The calculating program was written in PL/1 and run on a YeS computer.

Figures 1 and 2 [not reproduced] present curves for the change over time τ in thermal flow density ϕ and temperature t_c at the coating-substrate contact. Specific calculations were performed for precipitation of a TiN titanium nitride coating (λ=9 $Wm^{-1}\cdot K^{-1}$, a=2.15$\cdot 10^{-8}$ m^2/sec) on a substrate made of brass LS68 (λ=113 $Wm^{-1}\cdot K^{-1}$, a=34.6$\cdot 10^{-6}$ m^2/sec), when the substrate turns around the carousel axis at a constant angular velocity w=2 rpm. Coefficients in (1) were determined experimentally by probe measurements[8]. At I_g=60 A, U_B=-70 V; I_f=0 and residual gas pressure in the vacuum chamber P=6.6$\cdot 10^{-3}$ Pa. b_0, b_1, b_2 turned out to be equal to 4007.5, 2551, and 780.5. The values of other parameters included into equation (15) are: t_0=203 K; $\xi_0=10^{-8}$ m; $l=10^{-3}$, $5\cdot 10^{-3}$ and 10^{-2} m. The rate at which coating thickness increased, ω, varied within 10^{-3} and 10^{-8} m/sec.

These calculations show that thermal flow densities ϕ calculated at $\omega=10^{-8}$ and 10^{-5} m/sec differ slightly and trace the path described by the function $q(\tau)$ over time τ. Comparison of the results of calculation of temperature t_c at the coating application speeds mention shows that the discrepancy is no more than 5 percent. Only at $\omega=10^{-3}$ m/sec do conditions for heat exchange on the substrate-coating contact change because of the increase in coating thickness. Consequently, the substrate temperature field during ion-plasma coating

precipitation can be calculated without regard for condensation surface movement, since when coatings are applied by KIB method the precipitation rate does not exceed 10^{-8}-10^{-7} m/sec. Using averaged thermophysical and geometric coating parameters, one can simplify the statement of and solve thermal problems without a significant decrease in the accuracy of the results.

Figure 3 [not reproduced] illustrates the change in the condensation surface temperature for coating Y at time τ for different substrate thicknesses. The curves for $Y=Y(\tau)$ have segments where condensation surface temperature rapidly increases and then slows when the substrate crosses areas with maximum and minimum ion current densities. These segment indicate that substrate (and coating) temperature can be controlled by varying the carousel's angular rotation speed. Furthermore, the temperature of the substrate-coating system is stabilized by increasing the substrate's thickness, which, as the data show, has a significant effect on coating temperature.

References

1. V. V. Bedunkevich, M. B. Gordon, L. I. Mirkin, "Structure and Thickness of Titanium Nitride Ion-Plasma Coatings on High-Speed Steel," FIZIKA I KHIMIYA OBRABOTKI MATERIALOV, 1986, No. 3, pp. 57-64.

2. A. M. Darodnov, "Industrial Plasma Accelerators," ZhTF, 1078, 48, No. 9, p. 1858.

3. I. I. Aksenov, A. A. Andreyev, V. G. Bren, et al., "Coatings Produced by KIB Method (Plasma Flow Condensation in a Vacuum), UFN, 1979, 24, No. 4, pp. 515-525.

4. "Ionnaya implantatsiya," edited by J. K. Hirvonen. Moscow, 1985.

5. "Problemy teploobmena" [Problems of Heat Exchange]. Moscow, 1967, pp. 1-96.

6. Zh. A. Mrochek, A. B. Antonenko, A. L. Vershina, "Distribution of Temperature and Thermal Flows on the Substrate-Sublayer Contact During Electric Arc Application of Protective Coatings," ELEKTRONNAYA OBRABOTKA METALLOV, 1987, No. 1, pp. 23-26.

7. Zh. A. Mrochek, A. B. Antonenko, A. L. Vershina, "Temperature Fields for a Heterogeneous Substrate of Finite Thickness in Electric Arc Protective Coating Application Processes," ELEKTRONNAYA OBRABOTKA METALLOV, 1987, No. 6, pp. 16-20.

8. Zh. A. Mrochek, A. B. Antonenko, A. L. Vershina, "Density of a Thermal Flow Accumulated by a Substrate during Condensation of a Metal Plasma Flow," ELEKTRONNAYA OBRABOTKA METALLOV, 1989, No. 3, pp. 18-21.

9. B. N. Barabanov, I. G. Blinov, A. M. Dorodnov, et al., "High-Energy Plasma Technology Equipment -- 'Cold' Systems for Generating Plasma from Conductive Solids," FIZIKA I KHIMIYA OBRABOTKI MATERIALOV, 1978, No. 1, pp. 44-50.

Laser Heat Treatment With Oblique Beam Incidence

907D0028D Kishinev ELEKTRONNAYA OBRABOTKA MATERIALOV in Russian No 4, Jul-Aug 89 pp 25-27

[Article by A. N. Grechin, V. G. Korotkiy, I. R. Shlyapina, Moscow: "Laser Heat Treatment with Oblique Beam Incidence"]

[Text] Surface laser heat treatment of parts to increase their service properties has interested researchers, as can be seen in the large amount of published material. This material indicates that there are difficulties in laser treating the small-diameter interior cylindrical surfaces or the side surfaces of narrow groove and channels. In these cases, normal laser beam incidence on the surface cannot always be ensured, since the optical element (mirror) cannot be placed in a restricted space or its longevity is low.

Another problem in laser treatment is the widening of the hardening "track" when laser power is constant. Scanners which move the beam perpendicular to its main direction of travel or cylindrical optics are usually used. They make it possible to convert radiation with a round cross section into that with a rectangular cross section. These methods require special equipment, which is not always available to researchers.

These difficulties may be overcome if beam incidence is oblique to the surface. These irradiation conditions were reviewed in references 1 and 2. Authors were ordinarily limited to reporting that the size of the hardened zones is reduced basically by the decrease in depth when the angle of beam incidence increases. The goal of this work is a more detailed study of the effect of the angle of radiation incidence on the results of heat treatment.

Experiments were performed on specimens of steel 40Kh ready for shipment. An absorbent coating of MTsS-510 was applied to the surface of specimens measuring 20 x 30 x 60 mm with a spray painter[3] after grinding. A 2.5 kW Spectra Physics 973 continuous multimode CO_2 laser was used for laser treatment. The radiation did not have a primary polarization. It had a round cross section with uniform energy distribution. The radiation was focused with a KCl lens with a focusing distance of 550 mm.

Optimum heat treatment conditions were determined experimentally with a normal beam incidence at a power of P=1.5 kW and a spot diameter of 4.5 mm ($q=9\cdot10^3$ W/cm^2). The hardening zone was large (2b=4.3 mm; H=0.7 mm). At a beam speed of v=12.7 mm/sec the surface did not soften. Interaction time for the center of the "track" was τ=0.36 sec, which was defined as τ=d/v where d is beam

diameter. Power density and interaction time were the basic laser treatment parameters, and they remained unchanged in later experiments.

In experiments with normal beam incidence, treatment parameters were kept proportional to the change in the radiation power and spot area, spot diameter, and beam speed. Table 1 shows that the depth of the center of the hardening zone increases with spot area, while hardness remains unchanged (HRC=55).

Table 1. Effect of Radiation Focusing on Hardening Zone Parameters ($q=9\cdot10^3$ W/cm^2, τ=0.36 sec)

P, W	d, mm	v, mm/sec	Hardening "track", mm	
			Width B	Depth H
660	3.0	8.3	3.2	0.50
900	3.5	9.8	3.7	0.61
1200	4.0	11.2	4.1	0.67
1500	4.5	12.7	4.3	0.68
1850	5.0	14.0	5.0	0.73

Note: HRC=55.

With oblique beam incidence, the spot on the surface becomes an ellipse. Since radiation power was constant in these experiments, the focusing at each angle of slide (β) was adjusted to maintain spot area. Then the beam's speed was calculated according to the value for the ellipse's minor axis. The studies showed that the depth of the center of the hardening zone and its hardness were almost unchanged as beam slide angle was reduced (table 2). This was true even at β=14°, when "track" width was 9.8 mm.

Table 2. Effect of Angle of Slide on Hardening Zone Parameters (P=1.5 kW, $q=9\cdot10^3$ W/cm^2, τ=0.36 sec)

	Calculated length of ellipse axes, mm			Hardening "track"		
β°	Large 2b	Small 2a	v, mm/sec	B, mm	H, mm	HRC
90	4.5	4.5	12.7	4.3	0.7	55
75	4.6	4.4	12.3	4.6	0.7	54
60	4.8	4.2	11.7	4.8	0.6	54
45	5.3	3.8	10.7	5.7	0.7	55
40	5.6	3.6	10.0	6.6	0.7	54
30	6.4	3.2	8.8	6.8	0.7	50
20	7.7	2.6	7.3	8.2	0.7	55
14	9.1	2.2	6.2	9.8	0.6	53

With oblique beam incidence the energy absorbed by the specimens was determined by calorimetry. It was established that specimens acquire equal amounts of heat over equal periods of time. Consequently, the irradiated

surface's absorption coefficient does not depend on β. A similar result was obtain[4] when ANT-9A and ANT-17A absorptive flux pastes were used.

It seems that this effect is related to the structure of the absorptive coating applied to the metal. For this wave length (λ=10.6 microns) the size of the micro-irregularities and the distances between them cause a diffuse energy redistribution -- the surface is not a mirror, and the angle of slide becomes irrelevant.

To explain the results of the experiments on the basis of normal and oblique beam incidence, we performed thermal evaluations according to the procedure in reference 5. It was established that the thermal source in our experiments cannot be considered either a point or a surface. It has limited dimensions, and calculating temperature fields requires that the corresponding thermal problem be solved. With a normal beam incidence, the increase in hardening depth is apparently related to the increase in the area of the heat source and to the change in the shape of the heat front: from spherical to flat. With oblique radiation incidence, the area of the heat source was maintained, which explains why the depth of the hardening zone is constant.

A laser of relatively low power can thus be used to apply wide hardening "tracks" by changing the beam's angle of slide to 14°. To determine the effectiveness of this hardening method, a "track" 9.8 mm wide was produced using a one-dimensional scanner (f=52 Hz). Beam incidence was normal, and its diameter and travel speed matched those in the experiment with oblique incidence (P=1.5 kW, d=2a=2.2 mm, v=6.2 mm/sec).

The resulting "track" differed in shape from the preceding one: it's maximum depth was along the edges. This was attributable to the presence of dead spots during sinusoidal beam scanning. Hardening depth did not exceed 0.36 mm, which is much less than with oblique incidence (0.6 mm). Consequently, the same result (0.36 mm) with oblique incidence can be obtained at higher treatment rates.

Enlarging the area of a beam spot with constant power densities and interaction times increases the depth of the hardening zone. The use of absorptive coatings makes it possible to laser heat treat parts at angles of slide to 14° without changing the efficiency with which the radiation energy is used. When beam incidence is oblique, laser treatment productivity is much higher than when scanning devices are used.

References

1. G. J. Bruck, J. E. Smith, J. I. Nurminen, "A Study of the Effect of Angle of Beam Incidence on Laser Transformation Hardening of 4340 Alloy Steel," "ICALEO" 84: Proc. Mater. PRocess Symp. Boston Marriot/Copley Place, Nov. 12-15, 1984, LIA 44. Toledo, Ohio, 1985, pp. 120-132.

2. A. G. Grigoryants, A. N. Safonov, "Metody poverkhnostnoy lazernoy obrabotki" [Methods of Surface Laser Treatment]. Moscow, 1987.

3. V. P. Nikonarov, D. I. Roytenburg, "New Absorptive Coatings Used in Laser Hardening," TEKHNOLOGIYA MASHINOSTROYENIYA, 1982, No. 5, pp. 20-22.

4. V. A. Lopota et al., "Effectiveness of Treating Metals under Different Conditions for Interaction Between a CO_2 Laser and Surface," POVERKHNOST: FIZIKA, KHIMIYA, MEKHANIKA, 1983, No. 11, pp. 123-130.

5. A. A. Vedenov, G. G. Gladush, "Fizicheskiye protsessy pri lazernoy obrabotke materialov" [Physical Processes in Laser Treating Materials]. Moscow, 1985.

Electrochemical Treatment of Titanium Alloys, Trends in Its Development

907D0028E Kishinev ELEKTRONNAYA OBRABOTKA MATERIALOV in Russian No 4, Jul-Aug 89 pp 34-38

[Article by D. B. Chernyy, G. P. Prikhodko, O. A. Gorontiy, Kiev: "Electrochemical Treatment of Titanium Alloys and Trends in its Development"]

[Text] Electrochemical treatment (EKhO) of titanium and its alloys is a versatile process for producing parts with specified performance characteristics. Work on this problem is being done primarily to increase the strength of titanium and its alloys, increase the productivity of EKhO processes, and lower their cost. This report analyzes and defines the most important and promising trends in the development of EKhO processes for titanium alloys.

The most common processes for electrochemical treatment of titanium and its alloys are characterized by the use of solutions of strong mineral acids (HCl, H_2SO_4, HNO_3, HF) and their salts as electrolytes. The electrolyte is chosen depending on the purpose of the treatment: to increase hardness and wear resistance, improve adhesion, increase the surface cleanness class, produce anodic oxide films, or prepare the surface for different coatings. The most aggressive media for titanium are hydrofluoric acid and acid solutions containing fluorine ions. Titanium and its alloys are easily treated in solutions of alkaline metal halogenides, but are passivated in solutions of Na_2SO_4.

The same electrolytes continue to be used for EKhO of titanium and its alloys. In addition, it is noteworthy that the growing interest in electrolytes based on alcohols, organic acids (polyvinyl phosphonic, trifluormethylphosphonic), organic compounds, and weak inorganic acids (H_3BO_3, H_2SiO_3, H_3BF_6). As regards strong acids, there is interest in electrolytes based on orthophosphoric acid with various additives such as alkaline metal perchlorates, organize and hydroxy-acids, oxy-acid salts, etc. The use of electrolytes based on organic compounds is especially effective for electrochemical polishing of titanium. Electrolytes based on acid and glycerine are used in the tube industry and in machine manufacturing[1]. However the use of these electrolytes is linked to severe heating and high energy outlays.

The cleanness of the treated surface of titanium and its alloys during EKhO depends on several factors: the composition and temperature of the electrolyte, treatment time, and current density. The table shows electrolyte

The Use of Titanium Alloy EKhO Method in Industry

Electrolyte composition	Ti alloy grade	Temp., °C	Achievable surface cleanness	Operating conditions I-A/dm^2, U-B	Information source
Aqueous solution NaCl - 150 g/l, $NaNO_3$ - 30 g/l; KBr - 3 gl	TS5	20-22	∇5	I=200	[2]
Aqueous solution NaCl - 150 g/l $NaNO_3$ - 250 g/l; $NaNO_2$ - 30 g/l KBr - 3 g/l	TS5 VT3-1	80	∇5	I=10000-17000	[3]
Formamide solution of sulfaminic acid	VT1-0	20	∇7	I=25-175	[4]
Aqueous solution NaCl - 11% Na_2CO_3+NH_4NO_3 - 14%	VT3-1	70-80	∇7-9	U=20-25	[5]
Aqueous solution KCl - 100 g/l KBr - 100 g/l	VT1-0 VT22	35-40	∇6-7	I=5000	[6]
H_2SO_4 - 60-65%; HF - 20-25%; glycerine - 10-20%	VT9 VT16	25-35	∇7	I=70-200	[7]
H_2SO_4 - 9-44 g/l, H_3PO_4 - 7-36 g/l, NaCl - 5-30 g/l, TiO_2 - 1-15 g/l	VT20 VT16	60	∇7	I=0.5-1.5	[8]
CH_3COOH - 55-70 vol.% H_2SO_4 - 20-30 vol.% HF - 10-15 vol.% inhibitor 0.3-5 vol.%	VT14, VT9 VT3-1	40-50	∇4	I=0.01-0.5	[9]
H_2SO_4 - 1 mole/l $(NH_4)_2SO_4$ or Na_2SO_4 - 0.33 mole/l, soluble, bichromate, HF - 0.5-1.5 mole/l	OT4 OT4-0 OT4-1	50-80	∇5	I=10-100	[10]

compositions, electrical parameters, and other characteristics of certain EKhO processes used by industry. The increasing use of various additives to saline electrolytes and electrolytes based on strong acids to improve the effectiveness of the treatment process, lower the cost of the technology by reducing the use of scarce and expensive acids, especially sulfuric acid, and to ensure the safety of industrial treatment processes is noteworthy.

Study of nitrate, chlorate, and perchlorate solutions resulted in the development of electrolyte compositions for treating titanium and its alloys (VT1, VT5, VT3-1). It was concluded that chloric acid salts are promising electrolyte components. Adding them to a solution leads to electrochemical oxidation of the titanium to a low level of oxidation. Anode current density is from 0.2-20 A/cm^2; surface cleanness, class ∇7-8; and there is an

improvment in the titanium alloys' treatability[11]. Multi-ingredient solutions containing chlorides, bromides, nitrates, and nitrites of alkaline metals have also become common, although industrial use of multi-ingredient solutions is associated with individual difficulties related to the need to adjust electrolytes during use. It is in these electrolytes that titanium alloys are treated with high technological indicators. This is because titanium can be ionized to a low level of oxidation in multi-ingredient solutions and, consequently, from the standpoint of productivity multi-ingredient electrolytes are more promising: the removal rate increases, and the microgeometry of the surface layer improves[12].

Analysis of patent information reveals that the use of electrolytes based on phosphoric acid for titanium alloy polishing processes is promising: phosphoric acid has a low toxicity and aggressiveness, is cheaper than sulfuric acid, and more stable than organic acids.

Reference 13 proposed a method for electrochemical polishing of a wide range of metals, including titanium. In this method the electrolyzing solution contains a large amount of phosphoric acid and a small amount of an oxidizing ingredient, i.e. Ti_2O_3. It also contains Ni^{2+}, Fe^{3+}, and Cu^{2+} ions. The solution is stable and has low toxicity. Its use shortens electropolishing time and ensures high surface quality characteristics: shine, corrosion resistance, and high resistance to contamination.

Electrolytes based on phosphoric acid are also effective for removal metal coatings from titanium alloys. Removing coatings from worn parts has recently become an urgent problem. The removal of these metal coatings is important not only because of the scarcity or high cost of many rare metals, but also because of the cost of manufacturing parts and coatings. The increasing use of coated parts has made it necessary to re-use parts. However, the methods that have been developed are not always suitable, especially when one metal is to be removed from a multilayer coating. This problem was solved when a method was developed for electrolytic separation of one or several substrates in one operation[14] without damage to the surface and by minimum release of harmful vapors. The aqueous electrolyte includes HBF_4 (20-40 wt. percent) and phosphoric acid (5-25 wt. percent). The bath runs efficiently at room temperature, which minimizes harmful vapors. The solution's ingredients are inexpensive and stable, and the electrolyte requires no adjustment during operation. The solution efficiently removes copper-nickel and chrome coatings from the titanium surface. Current density is 1.5-4.5 A/cm^2 at a working voltage of 5-10 V.

Electrolytes based on phosphoric acid have also become widely used in our country[15-20].

The extensive use of titanium and its alloys in parts for new equipment requires increased part strength characteristics: microhardness, corrosion, heat, and wear resistance, and fatigue strength. For these purposes, part surfaces are anodized to produce oxide layers on a surface possessing particular properties. Furthermore, in several cases when titanium-based coatings are used, oxide layers must have good insulating characteristics -- high breakdown voltage, high resistance, as well as adhesive properties. Anodizing electrolytes sometimes include passivating ingredients -- magnesium chloride, sodium sulfate, ammonium molybdate, etc.

The strength, insulating, and adhesive properties of films depend on the thickness and, to a greater extent, on the structural uniformity of the oxide, which in turn depends on electrolyte composition and oxidizing conditions. A typical feature of the previous generation of EKhO processes is thick-layer anodizing, while at this stage processes ensuring thin films predominate. The good strength and insulating properties of thin oxide films are ensured by the more perfect structure of the oxide itself. An empirical equation for the growth of film thickness was found[21] when the process of thin-layer anodizing of alloy VT1-0 in a sulfuric acid solution with magnesium chloride added was studied.

Studies of the microhardness of titanium alloy surface layers after EKhO[22] showed that the increase in microhardness during the oxidation of parts made of titanium alloys VT9, VT20, and TI-2 is related to the penetration oxygen into the surface layer. Treatment was done in aqueous solutions of electrolytes with a ratio of $NaCl:NH_4NO_3=3:2$ and $NaCl:NaBr=1:1$. Microhardness in the first electrolyte was higher, 300-500 kgf/mm^2. Under optimum EKhO conditions, surface layer microhardness was 1.2-1.6 times higher than for the alloy in its initial state.

An oxide film with a resistance to 400-1000 mOhms is produced by anodizing titanium and its alloys in an aqueous electrolyte containing 1-5 percent alkaline metal silicate (sodium silicate), 1-3 percent alkaline metal perborate (sodium perborate), 1-5 percent diethyl-triamine-penta-acetic acid, and 25-96 percent water. Anodizing is done by applying a direct current increasing in time. The voltage application rate should not exceed 8 V/min. As a current density of 1.1-5.4 A/cm^2 is achieve, conditions stability and the part is held for 10-60 min. The film has elevated adhesion to the base and does not separate from the base even after the specimen has been in a chamber with 100-percent humidity at 30°C for 24 hr[23].

Pre-treatment of the metal surface before oxidizing is important, especially to obtain films firmly bonded to the base. The friction coefficient and resistance to abrasion are improved by pre-pickling the titanium in a solution containing 2 percent HF and 20 percent HNO_3 at 20°C, pickling rate 0.1 mm/hr; at 65°C, it is up to 0.2 mm/hr. This is followed by anodic oxidizing in a 2-percent aqueous solution of sulfuric acid at 20°C, voltage 15-20 V, for 15-20 min. The result is a porous oxide film with increased adhesion. To increase wear resistance, anodizing is done in a solution of several acids -- sulfuric, hydrochloric, nitric, and chloric -- at 48 V. Film thickness is 10 microns[24].

Study of AC polarization of titanium alloys made it possible to develop a process for diffusive electrochemical treatment (DEKhO) with industrial-frequency alternating current. Depending on the conditions and parameters for AC electrolysis on the surface of titanium alloys, oxide, oxide-hydride, or hydride layers differing in appearance, composition, stress-strain, and chemical properties are produced[19,20,25,26]. DEKhO can produce layers up to 40 microns thick which increase surface hardness by 200-300 kg/mm^2, do not separate or crack, and are characterized by a good friction coefficient (K_f=0.12 for a graphite ATG-VT5-1 pair). The hydrogen content in the surface layer after DEKhO decreases by an order of magnitude compared to the initial specimens. It was established that a titanium suboxide builds up in the surface layer of titanium alloys (VT5-1, VT22, OT4) during AC polarization. The crystal lattice of this suboxide is tightly bonded to the base and close

to the structure of the α-titanium matrix. Furthermore, metallographic studies demonstrated that solid solutions from the introduction of titanium hydride form in the surface layer on α-alloys of titanium after DEKhO of solid solutions. These solutions have a lamellar structure which leads to the formation of a structure like that of a composite material at a depth of 5-20 microns. Complex mechanical tests on specimens of alloys VT5L, VT5-1KT, and OT4 showed that the fatigue strength of parts treated by DEKhO remains unchanged or increases (OT4, VT22), and ductility properties and impact strength remain within initial limits. As electron microphotographs (using a Hitachi REM) of the relief of the surface of alloy VT5-1 after DEKhO show, phase distribution is more uniform and the alloy surface after DEKho is more even and smoother than an untreated one, i.e. the surface topography is more refined after DEKhO. The cleanness of surface treatment increases by a class, and the friction properties of the treated parts are improved.

In addition to such metal as aluminum, tantalum, and niobium, titanium and its alloys are used to produce capacitors, whose manufacturing process includes oxidation of the metal surface. To increase the structural uniformity and dielectric properties of anodic films and improve special parameters required in manufacturing high-quality electrolytic capacitors, titanium is anodized in an ethylene glycol electrolyte containing boric acid and ethylene glycol in a molar ratio of 1:1.5, 5:1.9, as well as a 10-30 wt. percent solution of ammonia. This solution is heated at 150-200°C for 5-20 min and diluted to 1-5 wt. percent in terms of the reaction product. This electrolyte is used at pH 4-8.5 and a voltage at 10-600 V. Anodizing is done in a reverse current with a reversing frequency of 10-130 per min[8].

A method for electrolytic application of coatings consisting of a mixture of titanium oxides and alkaline earth metals to titanium using alternating current has been proposed for manufacturing miniature high-capacitance electrostatic capacitors and circuits that trigger only upon an abrupt change in temperature, but are not sensitive to gradual changes, as well as corrosion-resistance housings and parts for machines. Electrolysis is done by three techniques: first for 0.5-2 hr at a current density of 50-100 ma/cm^2, then for 20 min at a current density of 100-150 mA/cm^2. The electrolyte is an aqueous solution of barium hydroxide. The coating has a high dielectric constant, as well as resistance and longevity[27].

Analysis of patent information revealed the following basic tendencies in the development of EKhO for titanium and its alloys: decreasing surface roughness, increasing strength properties (corrosion, heat, and wear resistance), improving electrical insulating properties of thin oxide films, increasing the rate of metal dissolution, reducing hydrogen absorption, lowering the energy consumed in treatment, and decreasing the surface friction coefficient. The most pressing are decreasing surface roughness or increase the cleanness class, and producing mirror-clean surfaces with high reflectivity. The most promising ways to do this are EKhO using a multi-component electrolytes that are inexpensive and contain chlorides and nitrates of alkaline metals as additives, electrolytes based on sodium chloride and potassium bromide containing orthophosphoric acid, and various organic additives.

The corrosion resistance of titanium and its alloys, as well as their strength characteristics are improved primarily by applying protective coatings through

anodizing. Electropolishing also strengthens the surface layer.

Hydrogen absorption by titanium and its alloys is diminished in various ways, including adding oxide components to the electrolyte to passivate the surface and thereby prevent hydrogen absorption, the addition of calcium chloride and sodium bichromate, as well as adjusting feed voltage. Furthermore, it is important to chose the electrolyte for treatment, since acid electrolytes promote greater hydrogen absorption by titanium and its alloys.

The use of EKhO in all stages of material processing -- from preparatory to finish tends to lower the process' energy consumption. This is done basically by selecting electrolyte compositions that make it possible to achieve good surface qualities with low electricity expenditures, e.g. those containing sodium nitrate and lithium chloride[28].

Organic electrolytes are promising in this regard. They require low current densities to achieve high surface cleanness. They are promising for EKhO because of the good treatability of the titanium and its alloys, especially to remove the oxide layer from the metal surface, which is hard to remove in inorganic solutions.

The problem of applying coatings to titanium and its alloys has resulted in a trend toward improving adhesion after electrochemical processing. This is achieved, for example, by treating the surface with alkaline solutions[29-31], aqueous solutions of soda, and hydrogen peroxide[32]. Pre-treatment -- degreasing, pickling, and activation -- which results in a strong bond between oxide and base, is important when the surfaces of titanium oxides are oxidized.

It is especially noteworthy that processes using industrial frequency alternating current, which are becoming increasingly common in all stages of titanium alloy treatment, are the most promising for reducing energy consumption and lowering the cost of EKhO processes.

References

1. N. V. Bogoyavlenskaya, "Electropolishing Titanium in Electrolytes Based on Organic Solvents," in "Khimicheskaya i elektrokhimicheskaya obrabotka prokata [Chemical and Electrochemical Treatment of Rolled Stock]. Dnepropetrovsk, 1974, pp. 28-29.

2. V. I. Mutsyanko, Ye. S. Stepanov, T. V. Kuleshova, "Use of Experiment Planning Methods for Selecting an Electrolyte during Electrochemical Processing of Titanium Alloy TS-5," ELEKTRONNAYA OBRABOTKA MATERIALOV, 1973, No. 2, pp. 89-91.

3. A. G. Marder, "Study of Surface Cleanness During Electrochemical Treatment of Titanium Alloys VT3-1 and TS-5," TRUDY TSNII TEKHNOLOGII MASHINOSTROYENIYA. Moscow, 1972, 103, pp. 46-55.

4. A. I. Gurashev, Ye. V. Rzhevskaya, "Electrochemical Polishing in a Formamide Solution of Sulfaminic Acid," Ibid., pp. 68-71.

5. USSR Author's Certificate 804334, class B 23 P 1/16. Electrolyte for

Dimensional Electrochemical Treatment of Titanium Alloys. Yu. A. Skvortsov. Published 2-15-81. BYUL. No. 6.

6. A. Sh. Bayramyan, "Kinetics of Anodic Dissolution of Titanium Alloys at High Current Densities," ELEKTRONNAYA OBRABOTKA MATERIALOV, 1982, No. 3, pp. 12-15.

7. USSR Author's Certificate 556925, class B 23 P 1/16. Electrolyte for Electrochemical Grinding of Titanium. V. M. Aparin, V. S. Limonov, E. L. Kanevskiy, et al. Published 5-5-77. BYUL. No. 17.

8. USSR Author's Certificate 476335, class C 23 B 9/00. Electrolyte for Anodizing Titanium Alloys. B. P. Batrakov, L. N. Pivovarova, A. S. Pivovarov, Published 7-5-75. BYUL. No. 25.

9. US Patent 3725224 Class IC^3 C 23 F 11/02. Composition for Electrolytic Descaling of Titanium and its Alloys. Earl W. Kendall. Published 6-30-71.

10. US Patent 3840442 Class C^3 C 23 F 11/02. Titanium or Titanium Alloys Having an Anodized Surface Layer and Method of Forming. Jacque André Chevalier. Published 4-7-72.

11. Yu. N. Petrov et al., "Study of Anodic Behavior of Titanium Alloys During EKhRO. 1. Nitrate, Chlorate, and Perchlorate Solutions," ELEKTRONNAYA OBRABOTKA MATERIALOV, 1983, No. 1, pp. 11-14.

12. N. D. Pronichev, "Study of Treatability of Titanium Alloys by Electrochemical Method," in "Progressivnyye metody elektrokhimicheskoy i elektrofizicheckoy obrabotki materialov" [Progressive Methods of Electrochemical and Electrophysical Treatment of Materials]. Ufa, 1979, pp. 44-46.

13. US Patent 3766030, Class 1 C^3 C 23 b 3/06, 1/100. Method of Electropolishing. Howard M. Greene. Canoga Park. Publ. 12-27.71.

14. US Patent 3793172, Class 1 C^3 b 01 K 3/00. Processes and Baths for Electro-Stripping Plated Metal Deposits from Articles. Charles T. Cadieux. Publ. 9-1-73.

15. USSR Author's Certificate 434139. Class C 23 b 3/10. Electrolyte for Electrochemical Polishing of Titanium and its Alloys. T. P. Maytak, N. D. Nazarenko. Publ. 6-30-74. BYUL. No. 24.

16. USSR Author's Certificate 463743. Class C 23 b 10. Electrolyte for Electrochemical Polishing of Titanium and its Alloys. T. P. Maytak, N. D. Nazarenko. Publ. 3-15-75. BYUL. No. 10.

17. USSR Author's Certificate 544667. Class C 25 F 3/08. Solution for Electrochemical Treatment of Titanium and its Alloys. A. V. Gorodyskiy, N. D. Nazarenko, V. M. Beletskiy, et al. Publ. 1-3-77. BYUL. No. 4.

18. USSR Author's Certificate 655494. Class B 23 P 1/04. Method of Electrochemical Treatment of Titanium Alloys. B. V. Borodin, A. V. Nikiforov, N. D. Pronichev, et al. Publ. 1-3-77. BYUL. No. 4.

19. USSR Author's Certificate 709720. Class C 25 D 11/26. Electrolyte for Anodizing Titanium and its Alloys. N. D. Nazarenko, I. D. Vdovenko, A. V. Gorodyskiy, et al. Publ. 1-15-80. BYUL. No. 2.

20. V. M. Beletskiy, N. D. Nazarenko, D. B. Chernyy, "Electrochemical Behavior of Titanium Alloys on Alternating Current," in "Dokl. X Ukr. resp. konf. po elektrokhimii [Papers of the 10th Ukrainian Republic Conference on Electrochemistry]. Kharkov, 1984, p. 102.

21. N. A. Marchenko, "Study of the Process of Deep Anodizing and Properties of Oxide Titanium Films," in "Metallicheskiye i nemetallicheskiye pokrytiya legkikh metallov i splavov [Metal and Nonmetal Coatings on Nonferrous Metals and Alloys]. Moscow, 1972, pp. 104-108.

22. O. A. Senina, "Effect of Electrolyte Composition on Gas Release and Their Penetration into the Surface Layer of Titanium Alloys," in "Elektrokhimicheskaya obrabotka detaley aviadvigateley [Electrochemical Treatment of Aircraft Engine Parts]. Kuybyshev, 1974, No. 1, pp. 61-66.

23. US Patent 3663379, Class C 23 b 11/02. Method and Electrolytes for Anodizing Titanium and its Alloys. Earl W. Kendall. Publ. 9-1-72.

24. French Application 2305629. Class F 16 B 11/00; C 09 5/02. Procéde de préparation de surface du titane et de ses alliages. Roland Romeo, Francois Villain. Published 3-28-75.

25. V. M. Beletskiy, D. B. Chernyy, N. D. Nazarenko, "Effect of AC Polarization on Surface Properties of Titanium Alloys," in "Fizikomekhanicheskiye svoystva galvanicheskikh i khimicheskikh pokrytiy metallami i splavami" [Physicomechanical Properties of Galvanic and Chemical Coatings]. Moscow, 1986, pp. 126-132.

26. V. M. Beletskiy, D. B. Chernyy, N. D. Nazarenko, "Diffusion Electrochemical Treatment of Titanium in Alternating Current," in "Khimicheskiye i elektrokhimicheskaya obrabotka poverkhnosti materialov" [Chemical and Electrochemical Treatment of Material Surfaces]. Kiev, 1985, pp. 76-77.

27. French Application 2240302. Class C 23 F 7/02. Procéde de traitement de piéces en titane ou es alliages de titane et piéces ainsi obtenues. Jean Maisonnier. Published 6-6-73.

28. Japanese Application No. 56-158894 C-25D 11/26. Tadao Nagata. Method of Anodic Oxidation of Titanium and Titanium Alloys. Published 12-7-81.

29. US Patent 3846261, Class 1 C^3 C 23 b 9/02; C 23 F 23/00. Anodizing et Metals. Karl Moeglich, Williams Ville. Publ. 9-6-72.

30. US Patent 3687741, Class 1 C^3 C 23 f 7/02. Method and Solutions for Treating Titanium and Like Metals and Their Alloys. Earl W. Kendall. Publ. 9-22-69.

31. US Patent 3907609, Class 1 C^3 C 23 C 1/10; C 23 F 7/24. Conversion Coating for Titanium and Titanium Base Alloys. Dolphus Harry Coggins. Publ.

2-14-69.

32. US Patent 4345969, Class 1 C^3 C 23 F 1/02; B 44 C 1/22; C 03 C 15/00; C 03 C 25/06. Metal Etch Solution and Method. Kristi L., James Phoenix, A. L. Shields. Publ. 3-23-81.

Hardening Steel in Electrolyte by Heating in Electrolytic Plasma

907D0028F Kishinev ELEKTRONNAYA OBRABOTKA MATERIALOV in Russian No 4, Jul-Aug 89 pp 43-46

[Article by V. N. Duradzhi, G. A. Fornya, Kishinev: "Hardening Steel in Electrolyte During Heating in Electrolytic Plasma"]

[Text] Heating metals and alloys in electrolytic plasma in an anodic process makes it possible to continuously change part temperature from 450 to 1000°C. The favorable combination of high heating temperature and the presence of the elements of an aqueous solution in an excited and ionized state in the gas-vapor sheath permits accelerated surface impregnation[1-3]. This work reviews the specific nature of metal hardening after surface impregnation with heating in an electrolyte.

The cooling rate for steel specimens during end heating in an electrolytic plasma was measured by oscillographing the temperature of cylindrical specimens 12 mm in diameter of steel 40Kh. Heating temperature was determined with a chromel-alumel thermocouple in the center of the specimen 2-2.5 mm from its base. Signals from the thermocouple traveled through a U7-2 DC amplifier to an H117/1 mirror galvanometer oscillograph.

When metal is heated in an electrolytic plasma during anodic and cathodic processes, a solid gas-vapor sheath exists around the active electrode. As a result, the following heat transfer stages should take place when steel parts are cooled in an electrolyte: film boiling, a transitional stage between film and nucleate boiling, nucleate boiling, and convection. On the anode temperature/time curves for hardening in various solutions used for surface impregnation these stages are identified by different cooling rates. After the electrical current is shut off, the solid gas-vapor sheath, i.e. developed film boiling, remains for a certain time, which varies from tenths of a second to several seconds and resulting from the physicochemical properties of the electrolyte, the initial temperature of the active electrode, and, to a great extent, solution temperature. The higher the solution temperature, the longer the continuous gas-vapor sheath remains, depending on the size of the active electrode and the composition and speed of the electrolyte in the area around the electrode. In this are, cooling rate is minimum -- 20-30 deg/sec. After the stable, continuous gas-vapor sheath has collapsed, at temperatures of 850-350°C the transitional boiling stage begins, and the gas-vapor sheath becomes discontinuous. Film boiling is accompanied by nucleate boiling. In this area the active electrode may come into contact with the electrolyte in certain places. The greatest temperature drop occurs here, and the cooling rate

varies from 300 to 500 deg/sec depending on electrolyte composition. When the temperature at which nucleate boiling is achieved, the cooling rate sharply drops to 20-30 deg/sec and remains at this level for 0.1-0.4 sec. The temperature at which nucleate boiling begins depends on the composition of the electrolyte. For a solution consisting of 15 percent ammonium chloride and 5 percent ammonium hydroxide, it is 320-330°C; for 15 percent ammonium chloride with 2.5 percent ammonium hydroxide and 10 percent acetone it is 28-300°C. For a solution consisting of 15 percent ammonium chloride and 10 percent acetone, the temperature of the transition to nucleate boiling is 240-260°C. The cooling rate is much lower in the nucleate boiling range, i.e. when anode temperature changes to 100-110°C, than in the previous stage, i.e. 80-140 deg/sec. At 100-110°C nucleate boiling stops and convective heat exchange begins, ensuring that the active electrode slowly cools to the temperature of the surrounding solution.

The effect of electrolyte composition on hardening rate makes it possible to explain the difference in the steels' mechanical properties after hardening in solutions containing 15 percent NH_4Cl and 5 percent NH_4OH or 15 percent NH_4Cl and 11 percent NH_4NO_4[4] despite their identical phase composition.

To arrive at a mathematical description of the hardening cooling of cylindrical specimens during end heating in electrolytic plasma, let us consider the two-dimensional axisymmetric problem of unstable heat conduction with nonlinear boundary conditions. The model of the active electrode and the area around it used for calculation appear in fig. 2 [not reproduced]. We will assume that film, transitional, and nucleate boiling and the conditions for convective heat transfer are established on the geometric boundaries of the active electrode. Disregarding heat release due to structure transformations in the steel, we will write the equation for thermal conductivity in the form

$$\partial T/\partial \tau = a(\partial^2 T/\partial r^2 + 1/r \cdot \partial T/\partial r + \partial^2 T/\partial z^2). \quad (1)$$

Initial conditions

$$\tau = 0;\ 0 \leq r \leq R;\ 0 \leq z \leq h;\ T = T_0. \quad (2)$$

Boundary conditions for the cylindrical surface and the cylinder's axis will be

$$\tau > 0;\ 0 \leq z \leq h; \begin{cases} r = R,\ \dfrac{\partial T}{\partial r} = \dfrac{-\alpha(T_n - t_c)}{\lambda}; \\ r = 0;\ \dfrac{\partial T}{\partial r} = 0. \end{cases} \quad (3)$$

On the base surface of the active electrode and in the cross section on the level of the solution surface

$$\tau > 0;\ 0 < r < R \begin{cases} z = 0;\ \dfrac{\partial T}{\partial z} = \dfrac{\alpha(T - t_c)}{\lambda}; \\ z = h;\ T = T^*; \end{cases} \quad (4)$$

where T_0, T, T_n, and T* are initial temperature, temperature on the axis of the active electrode and its surface, and temperature in the cross section on the level of the solution's surface; t_c, temperature of the surroundings,

equal to the saturation temperature t_s during film and nucleate boiling and electrolyte temperature t_e=20°C during convective heat transfer; boundaries between these conditions will be the nominal temperature at which nucleate boiling stops, which is defined by the equality of thermal flows during boiling and convection, 110°C; τ, time; a, λ, coefficients for the metal's thermal diffusivity and conductivity; α, coefficient of convective heat transfer on the cylinder's surface; r, R, current radius and cylinder radius; z, coordinate along the top of the cylinder counted from its base; h, cylinder height.

The coefficient of convective heat transfer during film boiling was determined by the following equation[5] with regard for the relationship of convective heat release intensity to solution temperature in the nucleus of the flow

$$\alpha_{n,n}=\lambda''\cdot\left[\frac{g\cdot(\rho'-\rho'')\cdot 2\cdot[\rho''\cdot H+\rho'\cdot c'\cdot(t_s-t_s)}{8\bar{n}^2[\mu''\cdot\lambda''\cdot(T_n-t_s)}\right]^{1/3}. \quad (5)$$

ρ' is the density of the liquid on the saturation line; λ'', μ'', coefficient of thermal conductivity and dynamic coefficient of vapor viscosity; ρ'', density of dry saturated vapor; H, vapor formation heat; g, gravitational acceleration.

The coefficient of convective heat release during the nucleate boiling of water is defined from the equation[6]

$$\alpha_{bub}=34.6(T_b-T_s)^{2.3} \quad (6)$$

The value of α_f was used in the range of T_{max} temperatures to 320°C, i.e. at the stages of film and transitional boiling; α_{bub}, in the temperature range from 320 to 110°C.

Problem (1)-(4) was solved on the basis of an explicit finite-difference scheme[7] with the following initial data: T_0=920, 850, and 700°C; R=6 and 10 mm; a = $10.6\cdot10^{-6}$ m^2/sec; α_{con}=1600 W/$m^2\cdot$K, $\lambda\doteq$40 W/m·K), α=5.6 W/$m^2\cdot$K. The intervals for the coordinates were $\Delta r=\Delta z\doteq$0.25 mm; in time, $\Delta\tau=5\cdot10^{-5}$ sec.

Calculating equations relating the temperature field and time in the active electrode show that the rate at which a specimen cools varies depending on boiling condition and that total cooling time is also a result of the active electrode's diameter. Calculating equations for the temperature field and experimental ones in the area for film boiling and transitional boiling are different because a value for α independent of time was used when the calculations were done, while under actual conditions it obviously changes over time from 180-200 to 1800 W/$m^2\cdot$K. Analysis of the results of calculations and comparison to experimental data make it possible to state that the rate of convective heat transfer in the film boiling stage is rather high and may be attributable to the temperature of the cooling solution in the nucleus of its flow.

The two-dimensional model (1)-(4) makes it possible to evaluate the effect of a part's non-isothermic surface on the duration of hardening cooling. The edge formed by the cylindrical surface and the end face cools more quickly than the rest of the surface. Analysis of the results shows that a wave of nucleate boiling spreads from the rapidly boiling edge over the end and

cylindrical surface.

References

1. B. R. Lazarenko, V. N. Duradzhi, A. A. Faktorovich, Ye. A. Pasinkovskiy, "Surface Impregnation of Metals by Electrical Discharges in Electrolytes during an Anodic Process," ELEKTRONNAYA OBRABOTKA MATERIALOV, 1974, No. 5, pp. 11-13.

2. V. N. Duradzhi, I. V. Bryantsev, Ye. A. Pasinkovskiy, "Carburizing and Nitrocarburizing of Steel During Heating in a Electrolytic Plasma," Ibid., 1977, No. 2, pp. 15-18.

3. V. N. Duradzhi, A. M. Mokrova, T. S. Lavrova, "Surface Impregnation of Steel in an Electrolytic Plasma," IZV. AN SSSR. SER. NEORGANICHESKIYE MATERIALY, 1985, 21, No. 9, pp. 1589-1591.

4. V. N. Aleksandrov, P. N. Belkin, Ye. A. Pasinkovksiy, et al., "Stress-Strain Properties of Steel 45 Nitrided in Electrolytic Plasma," ELEKTRONNAYA OBRABOTKA MATERIALOV, 1982, No. 2, pp. 17-18.

5. "Obshchiye i teoreticheskiye voprosy teploenergetiki. Gelioenergetika. Teploobmen pri plenochnom kipenii v elementakh energeticheskikh apparatov" [General and Theoretical Problems of Heat Engineering. Solar Power Engineering. Heat Transfer During Film Boiling in Power Engineering Equipment Elements], ed. V. K. Koshkin, vol. 3. Moscow, 1972.

6. V. I. Tolubinskiy, "Teploobmen pri kipenii" [Heat Transfer During Boiling]. Kiev, 1980.

7. A. A. Samarskiy, "Teoriya raznostnykh skhem" [Theory of Difference Schemes]. Moscow, 1983.

Electrochemical, Corrosion Behavior of Multilayer Coatings Based on Titanium Nitride

907D0028G Kishinev ELEKTRONNAYA OBRABOTKA MATERIALOV in Russian No 4, Jul-Aug 89 pp 52-55

[Article by A. M. Kotlyar, Ye. K. Sevidova, T. V. Steglik, Kharkov:
"Electrochemical and Corrosion Behavior of Multilayer Coatings Based on Titanium Nitride"

[Text] Titanium nitride's (TiN) high corrosion properties make it a promising material for use as a coating on items and parts subject to mechanical wear in aggressive media[1-4]. However, single-layer titanium nitride coatings produced by vacuum-plasma methods at thicknesses ensuring sufficient wear resistance and adhesive strength are porous and do not protect the base from the aggressive action of corrosive media.

One way to increase coated product corrosion resistance is to use multilayer coatings[5].

For this reason, the development of titanium nitride-based coatings seems promising. Because of the TiN, they would satisfy requirements for wear resistance, while their anti-corrosion properties would be strengthened by an interlayer of corrosion-resistant metal.

This work presents the results of studies of the effect of interlayers on the electrochemical and corrosion behavior of structures with TiN coatings for the medical and food industries.

The substrate materials were stainless steel 12Kh18N10T and galvanoplastic precipitates of nickel developed from a sulfamate electrolyte. Interlayers (of chromium) were applied galvanically and by vacuum plasma spray. Titanium nitride 5-6 microns thick was produced by plasma condensation during ion bombardment on a "Bulat-5T" setup.

Electrochemical studies (by measuring stationary potentials and plotting potentiodynamic polarization curves) were performed with a P-5848 potentiostat in a three-electrode cell at ambient temperature with natural solution aeration. The polarization rate was 1 mV/sec; the reference electrode was of chlorosilver. The electrolytes were a 3 percent solution of sodium chloride and 2 percent solutions of lactic and acetic acids.

The working specimens were dental appliances 17 mm in diameter. Before the experiment, the working surface (1 cm^2) was ground with emery paper, polished, and degreased with acetone and alcohol. Then it was rinsed in distilled water and dried. The specimens were fastened in a sealed organic glass holder with mechanical seal.

Corrosion studies were done by completely immersing the specimens into the test media at ambient temperature for 2,000 hr. The corrosion rate for stainless steel specimens was determined by weight method; for nickel-based specimens, according to the time at which the TiN coating began to separate.

Figures 1-3 [not reproduced] show potentiodynamic anodic and cathodic polarization curves for the solutions on specimens with stainless steel and nickel substrates. To compare the electrochemical behavior of the coated structures and the material of the coating itself, polarization curves are presented for TiN applied under identical conditions to a polycore substrate, which eliminates the effect of the metal base on the kinetics of electrode processes.

Results of Study of the Corrosion Rate and Stationary Potential in Model Media

Specimen material			2% solution 3% NaCl					
			Lactic acid				Acetic acid	
Base	Inter-layer	Outer layer	Cor. rate mc/cm^2/hr	St. pot. V	Cor. rate mc/cm^2/hr	St. pot. V	Cor. rate mc/cm^2/hr	St. pot. V
12Kh18N10T	-	-	$9.45 \cdot 10^{-5}$	+0.45	$4.64 \cdot 10^{-5}$	+0.18	$2.05 \cdot 10^{-5}$	0.52
12Kh18N10T	-	TiN	$5.40 \cdot 10^{-5}$	+0.52	$10.45 \cdot 10^{-5}$	+0.38	$4.64 \cdot 10^{-5}$	0.53
12Kh18N10T	Cr(g)	TiN	$9.29 \cdot 10^{-5}$	+0.52	$11.61 \cdot 10^{-5}$	+0.40	$8.13 \cdot 10^{-5}$	0.54
12Kh18N10T	Cr(v)	TiN	$8.13 \cdot 10^{-5}$	+0.50	$13.94 \cdot 10^{-5}$	+0.33	$11.61 \cdot 10^{-5}$	0.53

Extremely positive stationary potential values were observed for specimens with stainless steel substrates and the titanium nitride on the polycore in all solutions. These values correspond to the passive region, which is confirmed by very low corrosion rates (cf. table). The passivity region is retained over a rather wide range during anodic and cathodic polarization, especially in organic acid solutions from (-0.1)-(0) to (+0.8)-(+1.4) V. Application of titanium nitride to the stainless steel slowed both anodic and cathodic processes. The cathodic polarization curve for a structure with a single-layer coating almost matches that for titanium nitride. This is to be expected, since despite its porosity, the area of the titanium nitride is much larger than that of the steel in pores. The total kinetics of these systems is therefore governed by the kinetics of electrode reactions on the exterior layer. Therefore, the application of chromium interlayers had almost no effect on the rate of cathodic processes.

All curves for specimens with TiN coatings have a typical flat bend at potentials of (-0.4)-(-0.8). This area can probably be related to the change in the nature of cathodic reactions as potential shifts to the area of negative values.

The initial segments of the rise in cathodic current are related to the reduction of the dissolved oxygen according to reaction (1) and then to subsequent hydrogen release in reactions (2) and (3) in acid and sodium chloride solutions

$$O_2+4\bar{e}+4H^+=2H_2O \quad (1)$$

$$2H_3O^++2\bar{e}=H_2\uparrow+H_2O \quad (2)$$

$$2H_2O+2\bar{e}=H_2\uparrow+2OH^-. \quad (3)$$

As the curves show, the typical coefficients of Tafel segments vary depending on the pH of the solutions and the electrode material. According to the hypotheses of the authors of reference 6, electrochemical desorption may be a limiting stage in the process of hydrogen release on nitrides in acid media.

The specimens' anodic behavior differs more significantly depending on the materials included into the substrate/coating system and the nature of the corrosive medium. The effect of interlayers is ambiguous. In an NaCl solution, where the active increase in anodic current is related to pitting formation, the protective capacity of a coating of an interlayer of galvanic chromium 3-4 microns thick on steel 12Kh18N10T increases compared to single-layer coatings. A layer of vacuum chromium less than 1 micron thick is less effective against pitting corrosion. Anodic processes began at potentials above 0.8 V on all specimens with a TiN coating, i.e. after anodic reactions on the TiN began. They therefore reflect the total processes in the pores and on the material of the coating.

According to thermodynamic calculations[8], several kinds of oxidation reactions may take place on the surface of titanium nitride within this range of potentials:

$$2TiN+3H_2O=Ti_2O_3+N_2+6H^++6\bar{e}. \quad (4)$$

$$TiN+2H_2O=TiO_2+4H^+1/2N_2+4\bar{e}. \quad (5)$$

$$TiN=Ti^3+1/2N_2+3\bar{e} \quad (6)$$

$$TiN+3H_2O=Ti(OH)_3+3H^++1/2N_2+3\bar{e} \quad (7)$$

$$TiN+3H_2O=TiO_2\cdot H_2O+4H^++1/2N_2+4\bar{e} \quad (8)$$

The typical areas of current increase at potentials of (+0.8)-(+0.95), (+1.15)-(+1.30) and more than +1.5 V, as well as passivity areas corresponding among them are related to the consecutive reactions (4) and (5), which result in passivation (oxide formation) and transpassivation of the surface.

The range of stability for the steel and the titanium nitride is larger than in the chloride solutions in lactic acid. The anodic curves for the specimens are midway between the polarization curves for steel 12Kh18N10T and TiN. The galvanic chromium coating does not produce changes into the kinetics of the steel-TiN coating system, and the vacuum chromium even reduces polarization.

The depolarizing effect of chromium sublayers is more pronounced in acetic acid, probably due to the chromium's tendency toward transpassivation[7] which is intensified by the complex-forming properties of acetic acid. The acetic acid's aggressive action is seen in terms of titanium nitride -- the segment where anodic current rises begins at less positive values than for lactic acid -- at +0.7 and +1.4 V. The solution turns yellow in the anodic area, which points to the formation of soluble reaction products, mostly complex compounds of titanium with anions of acetic acid. Unlike lactic acid solutions, the polarization of the stainless steel-titanium nitride system takes place with a higher overvoltage than for the initial materials. This is probably related to the mutual effect of anodic material oxidation processes in the coating pores and in the coating itself.

Coating protective properties are improved when chromium interlayers are applied to galvanoplastic nickel substrates. Nickel dissolution potentials are much more negative than the beginning of oxidation reactions on titanium nitride. Cathodic in terms of nickel, coatings of chromium and titanium nitride protect a substrate mechanically, and the effective reduction of anodic current by 2-4 orders of magnitude between system corrosion potential and the beginning of anodic reactions on the interlayers is related primarily to the reduction in the number of through pores, cracks, and other defects.

Corrosion tests confirmed the results of electrochemical studies -- titanium nitride separated on specimens with single-layer coatings in acetic acid after 4 hr; in lactic acid in 26 hr. There was no separation throughout the tests (1440 hr) with coatings of vacuum and galvanic chromium. Visual inspection revealed that certain specimens had areas with lighter and darker TiN coatings, which indicate redox reactions around the pores.

A TiN coating slows cathodic reactions in acid solutions and, to a certain extent, in sodium chloride for both stainless steel and nickel substrates. The application of interlayers produces almost no change in the kinetics of hydrogen release. All cathodic curves for nitride-containing structures had a typical flat turn at potentials of (-0.4)-(-0.8) V, just as did steel substrate specimens.

Conclusions. 1. A 5-6-μ-thick titanium nitride coating applied by vacuum plasma method to a substrate of stainless steel 12Kh18N10T and of galvanoplastic nickel slows anodic and cathodic processes in solutions of organic acids and sodium chloride.

2. Interlayers of chromium applied to a nickel substrate effectively slow corrosive and anodic processes by lowering the active dissolution current by 2-4 orders of magnitude in all solutions studied.

3. The application of interlayers of chromium precipitated galvanically or by vacuum produces almost no change in the kinetics of cathodic processes in the metal-titanium nitride system.

4. Chromium sublayers produce no significant change in the corrosive or anodic behavior of systems with substrates of steel 12Kh18N10T in a solution of lactic acid, slightly increase their protective capability by shifting pitting formation potential to the positive region in sodium chloride, and reduce anodic polarization in acetic acid.

References

1. N. D. Tomashov, T. V. Chukalovskaya, I. L. Medova, F. F. Yegorov, "Corrosive and Anodic Behavior of Titanium Carbide, Nitride, and Boride in Sulfuric and Phosphoric Acid Solutions," ZASHCHITA METALLOV, 1985, 21, No. 5, pp. 682-688.

2. A. A. Trufanov, K. B. Katsov, V. N. Zhitomirskiy, "Corrosive-Electrochemical Properties of VT1-0 Alloy with Nitride Coatings in Acid Solutions," Ibid., 1988, 24, No. 1, pp. 127-129.

3. N. G. Boriskina, Ye. M. Kenina, T. A. Tumanova, et al., "Effect of Nitriding on the Resistance of Titanium Alloys AT3 and AT6 to Corrosion and Wear," Ibid., 1983, 19, No. 1, p. 61.

4. K. B. Katsov, A. A. Trufanov, V. N. Zhitomirskiy, "Effect of Titanium Nitride Coating on Low-Cycle Fatigue in Titanium Alloys VT1-1 and AT3 in a Corrosive Medium," FIZIKO-KHIMICHESKAYA MEKHANIKA MATERIALOV, 1985, 21, No. 3, pp. 102-103.

5. "Galvanicheskiye pokrytiya v mashinostroyenii" [Galvanic Coatings in Machine Building]. Vol. 2, 2-volume reference edited by L. D. Shluger. Moscow, 1985, p. 248.

6. V. A. Lavrenko, L. N. Yagupolskiy, Ye. V. Kozachenko, "Overvoltage in Hydrogen Release on Zirconium, Titanium, and Tantalum Nitrides om 1 N H_2SO_4," ELEKTROKHIMIYA, 1973, 19, No. 4, pp. 474-477.

7. "Korroziya i zashchita ot korrozii" [Corrosion and Corrosion Protection]. Vol. 1, edited by I. L. Rozenfeld, A. V. Byalobezhskiy. Moscow, 1971, p 264.

8. A. K. Gorbachev, "Thermodynamics of Redox Equilibria in TiN-H_2O Systems," ZASHCHITA METALLOV, 1983, 19, No. 2, pp. 253-256.

- END -

10

22161
57

NTIS
ATTN: PROCESS 103
5285 PORT ROYAL RD
SPRINGFIELD, VA 22161

Foreign Broadcast Information Service (FBIS) and Joint Publications Research Service (JPRS) publications contain political, economic, military, and sociological news, commentary, and other information, as well as scientific and technical data and reports. All information has been obtained from foreign radio and television broadcasts, news agency transmissions, newspapers, books, and periodicals. Items generally are processed from the first or best available source; it should not be inferred that they have been disseminated only in the medium, in the language, or to the area indicated. Items from foreign language sources are translated; those from English-language sources are transcribed, with personal and place names rendered in accordance with FBIS transliteration style.

Headlines, editorial reports, and material enclosed in brackets [ ] are supplied by FBIS/JPRS. Processing indicators such as [Text] or [Excerpts] in the first line of each item indicate how the information was processed from the original. Unfamiliar names rendered phonetically are enclosed in parentheses. Words or names preceded by a question mark and enclosed in parentheses were not clear from the original source but have been supplied as appropriate to the context. Other unattributed parenthetical notes within the body of an item originate with the source. Times within items are as given by the source. Passages in boldface or italics are as published.

SUBSCRIPTION/PROCUREMENT INFORMATION

The FBIS DAILY REPORT contains current news and information and is published Monday through Friday in eight volumes: China, East Europe, Soviet Union, East Asia, Near East & South Asia, Sub-Saharan Africa, Latin America, and West Europe. Supplements to the DAILY REPORTs may also be available periodically and will be distributed to regular DAILY REPORT subscribers. JPRS publications, which include approximately 50 regional, worldwide, and topical reports, generally contain less time-sensitive information and are published periodically.

Current DAILY REPORTs and JPRS publications are listed in *Government Reports Announcements* issued semimonthly by the National Technical Information Service (NTIS), 5285 Port Royal Road, Springfield, Virginia 22161 and the *Monthly Catalog of U.S. Government Publications* issued by the Superintendent of Documents, U.S. Government Printing Office, Washington, D.C. 20402.

The public may subscribe to either hardcover or microfiche versions of the DAILY REPORTs and JPRS publications through NTIS at the above address or by calling (703) 487-4630. Subscription rates will be provided by NTIS upon request. Subscriptions are available outside the United States from NTIS or appointed foreign dealers. New subscribers should expect a 30-day delay in receipt of the first issue.

U.S. Government offices may obtain subscriptions to the DAILY REPORTs or JPRS publications (hardcover or microfiche) at no charge through their sponsoring organizations. For additional information or assistance, call FBIS, (202) 338-6735,or write to P.O. Box 2604, Washington, D.C. 20013. Department of Defense consumers are required to submit requests through appropriate command validation channels to DIA, RTS-2C, Washington, D.C. 20301. (Telephone: (202) 373-3771, Autovon: 243-3771.)

Back issues or single copies of the DAILY REPORTs and JPRS publications are not available. Both the DAILY REPORTs and the JPRS publications are on file for public reference at the Library of Congress and at many Federal Depository Libraries. Reference copies may also be seen at many public and university libraries throughout the United States.